

University of California – Davis

UCD-96-24  
MADPH-96-969  
October, 1996

# Detecting and Studying $e^+e^- \rightarrow H^0 A^0; H^\pm H^\mp$ in the MSSM : Implications of Supersymmetric Decays and Discriminating GUT Scenarios

John F. Gunion

Davis Institute for High Energy Physics  
Department of Physics, University of California, Davis, CA 95616

James Kelly

Davis Institute for High Energy Physics  
Department of Physics, University of California, Davis, CA 95616  
and  
Department of Physics, University of Wisconsin, Madison, WI 53706

## Abstract

We demonstrate that supersymmetric decays, as typified by the predictions of several GUT-scale boundary condition choices, do not prevent detection of  $Z^0 \rightarrow H^0 A^0; H^\pm H^\mp$ , at a 1 TeV–4 TeV  $e^+e^-$  or  $\mu^+\mu^-$  collider operating at anticipated luminosity. For much of parameter space the relative branching ratios for various SUSY and non-SUSY decays can be measured with sufficient accuracy that different GUT-scale boundary condition choices can be distinguished from one another at a very high confidence level.

## 1 Introduction

The minimal supersymmetric model (MSSM) is widely regarded as the most attractive extension of the Standard Model (SM). The approximate unification of coupling constants that occurs in the MSSM at an energy scale of a few times  $10^{16}$  GeV [1] suggests the appropriateness of treating the MSSM in the context of a grand unified (GUT) model, in which the supersymmetry breaking parameters have simple universal values at the unification scale,  $M_U$ . The GUT framework is especially compelling in that electroweak symmetry breaking (EWSB) is easily induced at a scale  $\sim m_Z$  as the soft mass-squared of the Higgs field that couples to the top quark is driven to small (sometimes negative) values by the associated large Yukawa coupling during evolution to low energy scales. Thus, it is important to consider the implications of GUT scenarios for the detection of the Higgs bosons of the MSSM and to determine the extent to which (and strategies by which)

Higgs boson decay branching fractions can be measured with accuracy sufficient to constrain GUT models.

The Higgs sector of the MSSM is reviewed in Refs. [2, 3]. The MSSM contains exactly two Higgs doublets, leading to two CP-even Higgs bosons ( $h^0$  and  $H^0$ , with  $m_{h^0} < m_{H^0}$ ), one CP-odd Higgs boson ( $A^0$ ) and a charged Higgs pair ( $H^\pm$ ). Crucial parameters for the Higgs sector are  $m_{A^0}$  and  $\tan\beta$  (the ratio of the vacuum expectation values for the neutral Higgs fields that give mass to up-type and down-type quarks, respectively). A fundamentally important GUT result is that essentially all models with proper EW SB require  $m_{A^0} > 200$  GeV, with much larger values being common. This result has many important implications:

The  $h^0$  will be very SM-like, and, at fixed  $\tan\beta$ , will have a mass near the upper bound predicted by including (two-loop/RGE-improved) radiative corrections as computed for the known value of  $m_t$  and the values for stop-squark masses and mixing predicted by the GUT. For all scenarios considered (even those with  $m_{A^0}$  well above a TeV),  $m_{h^0}$  is below 130 GeV and, as reviewed in Ref. [3], will be discovered with relative ease at both the LHC and any  $e^+e^-$  or  $p\bar{p}$  collider with  $\sqrt{s} > 500$  GeV. However, because the  $h^0$  will be very SM-like, it will be quite difficult to establish on the basis of precision measurements that it is the MSSM  $h^0$  and not the SM Higgs, especially if  $m_{A^0} > 300 - 400$  GeV [3].

The  $H^0$ ,  $A^0$  and  $H^\pm$  will be approximately degenerate in mass and will decouple from the vector boson sector. The coupling of the  $A^0$  to  $b\bar{b}$  [ $t\bar{t}$ ] is given by 5 times  $g_{b^0} = (2m_W)\tan\beta$  [ $g_{t^0} = (2m_W)\cot\beta$ ]. For large  $m_{A^0}$ , the couplings of the  $H^0$  asymptote to 1/5 times these same coefficients. The  $H^\pm \rightarrow t\bar{b}$  coupling is proportional to  $ig = (2m_W)(m_{bP_R}\tan\beta + m_{tP_L}\cot\beta)$ .

In most GUT scenarios, the high masses predicted for the  $H^0$  and  $A^0$  imply that decays to pairs of supersymmetric particles will be important when  $\tan\beta$  is not large and  $t\bar{t}$  decays are not kinematically allowed. For small to moderate  $\tan\beta$  and  $m_{H^0}, m_{A^0} > 2m_t$ ,  $t\bar{t}$  is the dominant mode unless the mass of the lightest stop squark,  $\tilde{t}_1$ , is small enough that decays to  $\tilde{t}_1\tilde{t}_1$  are kinematically allowed. (This does not happen in the GUT models we consider.) When  $\tan\beta$  is large, the enhanced  $b\bar{b}$  coupling of the  $A^0$  and  $H^0$  imply that  $b\bar{b}$  decays will become dominant, even when SUSY and/or  $t\bar{t}$  decay modes are allowed. In the case of the  $H^\pm$ , SUSY decays always compete with the larger  $t\bar{b}$  decay mode since  $m_H > m_t + m_b$  for the GUT scenarios considered. (In the GUT models we consider,  $\tilde{t}_1\tilde{b}_1$  decays are not kinematically allowed.)

For  $m_{A^0} > 200$  GeV it is entirely possible that none of these heavy Higgs bosons could be detected at the LHC (see the review of Ref. [3]), even assuming the absence of SUSY decays. In terms of the  $(m_{A^0}, \tan\beta)$  parameter

space plane, heavy Higgs discovery is not possible once  $m_{A^0} > 200 \text{ GeV}$  if  $\tan \beta > 3$  and if  $\tan \beta$  lies below an upper limit that increases with increasing  $m_{A^0}$  (reaching  $\tan \beta = 15$  by  $m_{A^0} = 500 \text{ GeV}$ , for example). More than likely, the  $\tan \beta < 3$  discovery region would be diminished after including the SUSY decays of the  $H^0$  and  $A^0$  that are predicted to be important. Detection of the  $H^0$  and  $A^0$  via such SUSY decays at the LHC appears to be very difficult except in rather special situations.

The only large rate production modes for these heavy Higgs bosons at an  $e^+e^-$  or  $pp$  collider will be  $Z^0 \rightarrow H^0 A^0$  and  $Z^0 \rightarrow H^\pm H^\mp$ . These modes are kinematically limited to  $m_{A^0} - m_{H^0} - m_H < \sqrt{s}/2$ . In particular, at a first  $e^+e^-$  collider with  $\sqrt{s} = 500 \text{ GeV}$  and  $L = 50 \text{ fb}^{-1}$  observation is restricted to roughly  $< 220 - 230 \text{ GeV}$ , implying that detection would not be possible in most GUT scenarios.

Although single  $H^0$  and  $A^0$  production is significant at a  $pp$  collider facility for masses  $< 0.8 \sqrt{s}$ , i.e. about  $400 \text{ GeV}$  at a  $\sqrt{s} = 500 \text{ GeV}$   $e^+e^-$  collider, backgrounds are such that very high luminosities are required for discovery [4] |  $L > 200 \text{ fb}^{-1}$  is required when either SUSY decays are significant or  $\tan \beta$  is large.

In combination, these results imply that  $H^0$ ,  $A^0$ , and  $H^\pm$  detection may very well require employing the  $Z^0 \rightarrow H^0 A^0$  and  $Z^0 \rightarrow H^\pm H^\mp$  production modes at an  $e^+e^-$  or  $pp$  collider with  $\sqrt{s}$  substantially above  $500 \text{ GeV}$ . Even if the  $H^0$  and  $A^0$  are observed at the LHC, studying their decays and couplings would be much simpler in the pair modes. Various aspects of Higgs pair production are discussed in Ref. [5], which appeared as we were completing the present work.

Our first goal is to determine the luminosity required to guarantee observability of the  $Z^0 \rightarrow H^0 A^0$ ;  $H^\pm H^\mp$  modes regardless of the SUSY-GUT decay scenario. We will consider collider energies of  $1 \text{ TeV}$  and  $4 \text{ TeV}$  (the latter being actively considered [6] for  $pp$  colliders), with integrated luminosities up to  $200 \text{ fb}^{-1}$  and  $1000 \text{ fb}^{-1}$ , respectively. Our second goal will be to develop strategies for organizing the rates observed for physically distinct final states so as to yield information regarding the relative branching fractions of different types of decay modes, and to assess the extent to which such information can determine the GUT scenario and its parameters given the expected experimental errors.

We find that if the integrated luminosity at  $1 \text{ TeV}$  ( $4 \text{ TeV}$ ) is close to  $200 \text{ fb}^{-1}$  ( $1000 \text{ fb}^{-1}$ ) then detection of the  $H^0 A^0$  and  $H^\pm H^\mp$  pair production processes will be possible over almost all of the kinematically allowed parameter space in the models we consider, but that significant reductions in these luminosities will imply gaps in parameter space coverage. A measurement of the mass  $m_{A^0} - m_{H^0} - m_H$  already provides critical constraints on the GUT model. The correlation between this mass and the masses of the charginos, neutralinos, and/or sleptons (as measured in direct production) determines the GUT scale boundary conditions

(provided there is universality for the standard soft-SUSY-breaking parameters) and a fairly unique location in the parameter space of the GUT model so singled out. In particular,  $\tan\beta$  is determined. Assuming full luminosity, the relative Higgs branching fractions can be used to cross check the consistency of the GUT model and confirm the parameter space location with substantial precision. For example, the relative branching fractions for the  $H^0; A^0; H^\pm$  to decay to SUSY pair particle states vs. Standard Model pair states provide a surprisingly accurate determination of  $\tan\beta$  given a measured value for  $m_{A^0}$ . This  $\tan\beta$  value must agree with that determined from the masses. Other relative branching fractions provide complementary information that can be used to further constrain the GUT model, and can provide a determination of the sign of the Higgs superfield mixing parameter. Thus, a relatively thorough study of the full Higgs sector of the MSSM will be possible and will provide consistency checks and constraints that could single out the correct GUT model.

The organization of the paper is as follows. In the next section, we describe the six GUT models that we consider, and delineate the allowed parameter space for each. Contours of constant Higgs boson, neutralino and chargino masses are given within the allowed parameter space, and Higgs boson decay branching fractions are illustrated. In Section 3, we demonstrate that, for expected integrated luminosities at  $e^+e^-$  or  $pp$  colliders, detection of Higgs pair production will be possible in final states modes where both Higgs bosons decay to final states containing only b or t quarks, even though the branching fractions for such final states are decreased due to competition from the SUSY decay channels. Event rate contours as a function of parameter space location are presented for the six GUT models. In Section 4, we determine the prospects for measuring the branching fractions for various Higgs boson decays, including those for specific supersymmetric (SUSY) sparticle pairs. The ability to discriminate between different GUT models and to determine the parameter space location within the correct GUT model on the basis of Higgs decays is delineated. Section 5 summarizes our results and conclusions.

## 2 The GUT Models, Masses and Higgs Decays

In the simplest GUT treatments of the MSSM, soft supersymmetry breaking at the GUT scale is specified by three universal parameters:

- $m_0$ : the universal soft scalar mass;
- $m_{1/2}$ : the universal soft gaugino mass;
- $A_0$ : the universal soft Yukawa coefficient.

The absolute value of  $\mu$  (the Higgs mixing parameter) is determined by requiring that radiative EW SB gives the exact value of  $m_Z$  for the experimentally measured

value of  $m_t$ ; however, the sign of  $\tan\beta$  remains undetermined. Thus, the remaining parameters required to completely fix the model are

$\tan\beta$ : the vacuum expectation value ratio; and

$\text{sign}(\mu)$ .

We remind the reader that a universal gaugino mass at the GUT scale implies that  $M_3:M_2:M_1 = 3:1:1=2$  at scale  $m_Z$ . For models of this class one also finds that  $j = j = M_{1/2}$ . These two facts imply that the  $e_1^0$  is mainly bino, while  $e_2^0$  and  $e_1^+$  are mainly wino, with heavier gauginos being mainly higgsino [7]. The running gluino mass  $m_{\tilde{g}}$  ( $m_{\tilde{g}}$ ) is roughly three times as large as  $m_{e_2^0} = m_{e_1^+}$  which in turn is of order twice as large as  $m_{e_1^0}$ . (The pole gluino mass is generally substantially larger than  $m_{\tilde{g}}$  ( $m_{\tilde{g}}$ ) when squark masses are large.)

We will consider three representative GUT scenarios characterized by increasingly large values of  $m_0$  relative to  $m_{1/2}$  (which translates into increasingly large slepton masses as compared to  $m_{e_1^0}$ ,  $m_{e_2^0}$ , and  $m_{e_1^+}$ ):

"No-Scale" (NS) [8]:  $A_0 = m_0 = 0$ ;

"Dilaton" (D) [9]:  $m_{1/2} = A_0 = \frac{p}{3} m_0$ ;

"Heavy-Scalar" (HS):  $m_0 = m_{1/2}$ ,  $A_0 = 0$ .

Within any one of these three scenarios, the model is completely specified by values for  $m_{1/2}$ ,  $\tan\beta$  and  $\text{sign}(\mu)$ . We will present results in the  $(m_{1/2}; \tan\beta)$  parameter space for a given  $\text{sign}(\mu)$  and a given choice of scenario. Our notation will be NS for the No-Scale scenario with  $\text{sign}(\mu) < 0$ , and so forth.

In Figures 1, 2, and 3 we display the allowed  $(m_{1/2}; \tan\beta)$  parameter space for the NS, D and HS scenarios, respectively. The boundaries of the allowed parameter space are fixed by experimental and theoretical constraints as follows:

The left-hand boundary at low  $m_{1/2}$  derives from requiring that  $Z \rightarrow \text{SUSY}$  decays not violate LEP1 limits.

The low- $\tan\beta$  boundary is obtained by requiring that the t-quark Yukawa coupling remain perturbative in evolving from scale  $m_Z$  to the GUT scale.

In the NS scenario, the allowed parameter space is finite by virtue of two competing requirements. First, there is an upper bound on  $\tan\beta$  as a function of  $m_{1/2}$  obtained by requiring that the LSP (always the  $e_1^0$  in the allowed region) not be charged (i.e. we require  $m_{e_1} = m_{e_1^0}$ ).<sup>1</sup> Second, there is the lower bound on  $\tan\beta$  required by t-quark Yukawa perturbativity. One finds that for large enough  $m_{1/2}$  the upper bound drops below the lower bound.

---

<sup>1</sup>This bound is especially strong in the NS scenario due to the fact that  $m_0 = 0$  implies very modest masses for the sleptons, in particular the  $e_1$ , at scale  $m_Z$ .

The upper bound on  $\tan\beta$  as a function of  $m_{1=2}$  in the D scenario comes from demanding that the LSP not be charged.

In the HS scenario, the upper bound on  $\tan\beta$  arises by requiring that the SM-like light Higgs mass lie above the current limit of  $m_{h^0} > 63 \text{ GeV}$ . (In the HS scenario, for fixed  $m_{1=2}$ ,  $m_{A^0}$  becomes smaller and smaller as  $\tan\beta$  increases until eventually it approaches zero forcing  $m_{h^0}$  to decline rapidly. In other scenarios, with lighter scalar masses and hence sleptons, the LSP becomes charged before  $\tan\beta$  becomes so large that  $m_{A^0}$  starts declining rapidly.)

In the D and HS scenarios, there is no upper bound on  $m_{1=2}$  unless cosmological constraints are imposed. High  $m_{1=2}$  values (roughly,  $m_{1=2} > 500 \text{ GeV}$  [10]) are, however, disfavored by naturalness considerations.

Before proceeding, we provide a few technical notes. First, we note that the evolution equations must be implemented very carefully when considering very large  $m_{A^0}$  values. In order to avoid instabilities<sup>2</sup> deriving from unnaturally large (and hence unreliable) one-loop corrections (for going from running masses to pole masses), we found it necessary to terminate evolution for soft masses at scales of order the associated physical squark, slepton and heavy Higgs masses. In this way, the one-loop corrections are kept small and the physical masses obtained are reliable. The evolution program we employed is based on one developed by C. H. Chen [12]. Results at low mass scales were checked against results obtained using the programs developed for the work of Refs. [13] and [4]. Once the appropriate low-energy parameters were determined from the evolution, we then employed ISASUSY [11] to obtain the branching ratios for the Higgs boson and subsequent chain decays. The ISASUSY results were cross-checked with our own programs. The decay results were then combined with Higgs boson pair production rates to determine rates for specific classes of final states.

## 2.1 Sparticle and Higgs Masses

Also displayed in Figs. 1, 2, and 3 are contours of constant  $m_{\tilde{e}_1^0}$ ,  $m_{\tilde{e}_1^+}$ ,  $m_{\tilde{e}_R}$ , and  $m_{A^0}$ . These reveal the importance of detecting the heavy Higgs bosons and measuring their masses accurately. The masses of the inos and the sleptons will presumably be measured quite accurately, and the figures show that they will determine in large measure the values of  $m_{1=2}$  and  $m_0$ . But the rather vertical nature of the  $m_{\tilde{e}_1^0}$ ,  $m_{\tilde{e}_1^+}$ , and  $m_{\tilde{e}_R}$  contours implies that  $\tan\beta$  is likely to be poorly determined from these masses alone. Fortunately, the  $m_{A^0}$  contours are not nearly so vertical, implying that a measurement of  $m_{A^0}$  can be combined with the  $m_{1=2}$  determination from the ino masses to fix a value of  $\tan\beta$ . The accuracy of this

---

<sup>2</sup>Such instabilities are found, for example, in ISASUGRA [11].

## No Scale Scenario Mass Contours (GeV)

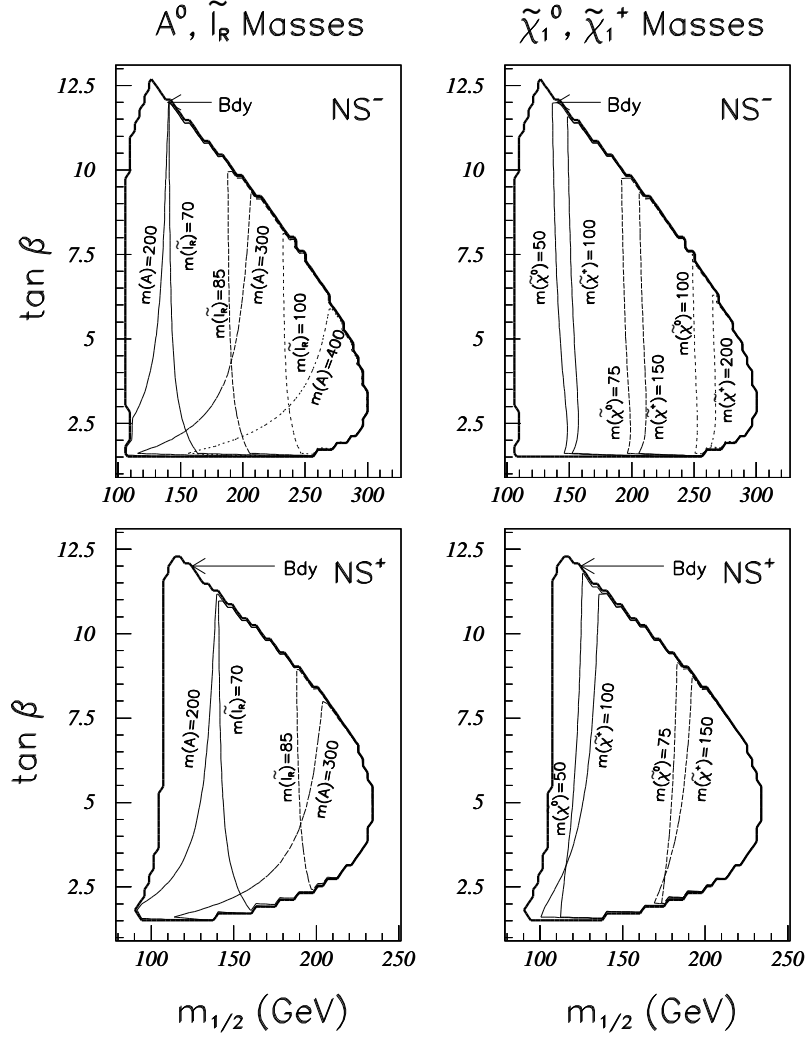


Figure 1: We show the  $(m_{1/2}, \tan \beta)$  parameter space regions (bold outer perimeter) within which we find a consistent EW SB solution for the No-Scale model. Contours of constant mass are shown within the allowed region for the  $\tilde{e}_1^0, \tilde{e}_1, A^0$  and  $\tilde{e}_R$ . Results for both signs of  $\mu$  are shown.

## Dilaton Scenario Mass Contours (GeV)

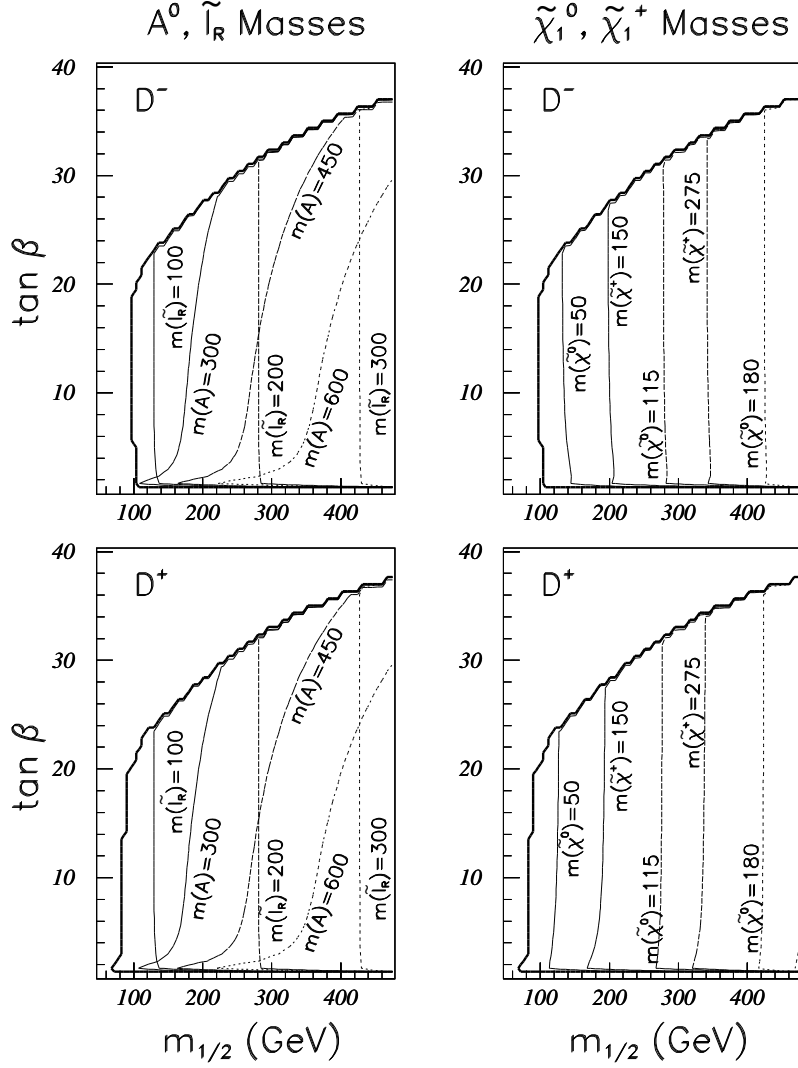


Figure 2: We show the  $(m_{1/2}, \tan \beta)$  parameter space regions (bold outer perimeter) within which we find a consistent EW/SB solution for the Dilaton model. Contours of constant mass are shown within the allowed region for the  $e_1^0, e_1, A^0$  and  $\tilde{l}_R$ . Results for both signs of  $\mu$  are shown.

## Heavy Scalar Scenario Mass Contours (GeV)

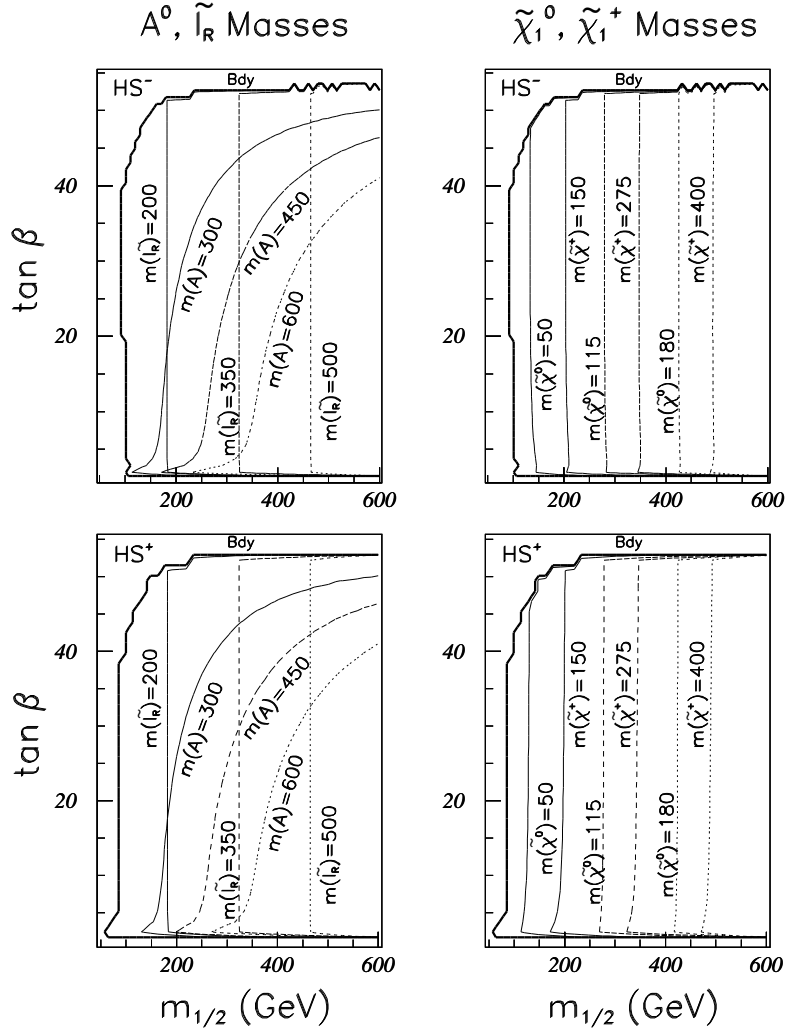


Figure 3: We show the  $(m_{1/2}, \tan \beta)$  parameter space regions (bold outer perimeter) within which we find a consistent EW SB solution for the Heavy-Scalar model. Contours of constant mass are shown within the allowed region for the  $e_1^0, e_1^\pm, A^0$  and  $\tilde{e}_R$ . Results for both signs of  $\mu$  are shown.

determination depends upon the accuracy with which  $m_{A^0}$  (and  $m_{H^0}, m_H$ ) can be measured. For discovery in the  $A^0 \rightarrow b\bar{b}$  decay mode (as possible for almost all model parameter choices at full luminosity, see later), this accuracy is fixed by the  $b\bar{b}$  mass resolution. At an  $e^+e^-$  collider, a resolution of  $\Delta M_{b\bar{b}} \approx 10 \text{ GeV}$  is probably attainable. For a large number,  $N$ , of events,  $m_{A^0}$  can be fixed to a value of order  $\Delta M_{b\bar{b}}/\sqrt{N}$ , which for  $N = 20$  (our minimal discovery criterion) would imply  $\Delta m_{A^0} \approx 2-3 \text{ GeV}$ . Examination of the figures shows that such mass uncertainty will lead to a rather precise  $\tan\beta$  determination within a given GUT model, except at low  $m_{A^0}$  and high  $\tan\beta$  in the NS case.

## 2.2 Higgs Decays

Let us now turn to the decays of the heavy Higgs bosons of the MSSM. As already noted, our ultimate goal is to use these to confirm/re-enforce the correctness of both the model and the parameter choices within the model that has been singled out by the mass measurements. The most important common feature of the GUT models we consider is that squarks are always sufficiently heavy that decays of Higgs bosons to squark pairs are not kinematically allowed. This is true even for the NS boundary conditions with  $m_0 = 0$ , in which the large squark masses derive from the substantial evolution of the colored soft-scalar masses to positive values as the scale decreases from  $M_U$  towards  $m_Z$ . In order that the squarks be light enough for squark pairs to appear in Higgs decays, substantial breaking of the universality of soft-SUSY-breaking scalar masses at the GUT scale is required. For example, light sbottom and stop squarks can be consistent with radiative EW SB via evolution if the Higgs soft scalar masses are much larger than the squark (in particular, stop and sbottom) soft scalar masses at  $M_U$ . In this case,  $H^0, A^0 \rightarrow \tilde{t}_1 \tilde{t}_1^*, \tilde{b}_1 \tilde{b}_1^*$  and  $H^\pm \rightarrow \tilde{t}_1 \tilde{b}_1^*$  pair channels would dilute the SM decay modes of the Higgs to a much greater extent than do the chargino and slepton decays in the models discussed here. Strategies for detecting and studying  $H^0 A^0$  and  $H^\pm H^\mp$  pair production would have to be reconsidered. In any case, there would be no difficulty in distinguishing models with light stop and/or sbottom squarks from the NS, D and HS models considered here.

In fact, the three models we consider are rather similar to one another in most respects. Thus, they provide a good testing ground for assessing the extent to which we can distinguish between models by using experimental information from the Higgs sector. We shall see that Higgs branching ratios depend substantially on the particular model choice and on the precise location in parameter space within a given model. Figures 4a, 4b, and 4c illustrate the dependence of Higgs branching fractions upon parameter space location for the  $\langle 0 | D | 0 \rangle$  (D) scenario. In these figures, we give contours of constant branching fractions for  $H^0, A^0$  and  $H^\pm$  decays. The decay channels  $b\bar{b}, t\bar{t}, e_1^+ e_1^-, e_1^0 e_2^0$ , and the sum over all SUSY decay channels, are considered for both the  $H^0$  and  $A^0$ . In addition, we show the  $h^0 h^0$  and  $ee$  (summed over all  $e$  types) branching fractions for the  $H^0$ . (The  $ee$

# Dilaton ( $\mu=-$ ) Branching Ratio Contours

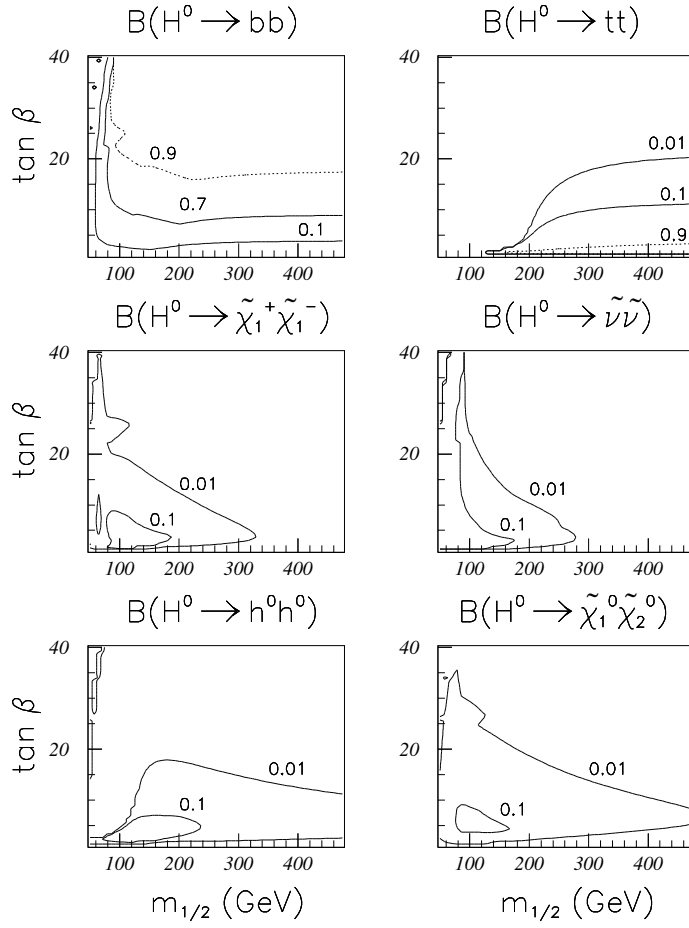


Figure 4: a) We show contours within the  $(m_{1/2}; \tan \beta)$  parameter space of constant branching fraction for the  $H^0 \rightarrow b\bar{b}, t\bar{t}, e_1^+ e_1^-, ee, h^0 h^0$ , and  $e_1^0 e_2^0$  decay channels. Results are for the D scenario.

# Dilaton ( $\mu=-$ ) Branching Ratio Contours

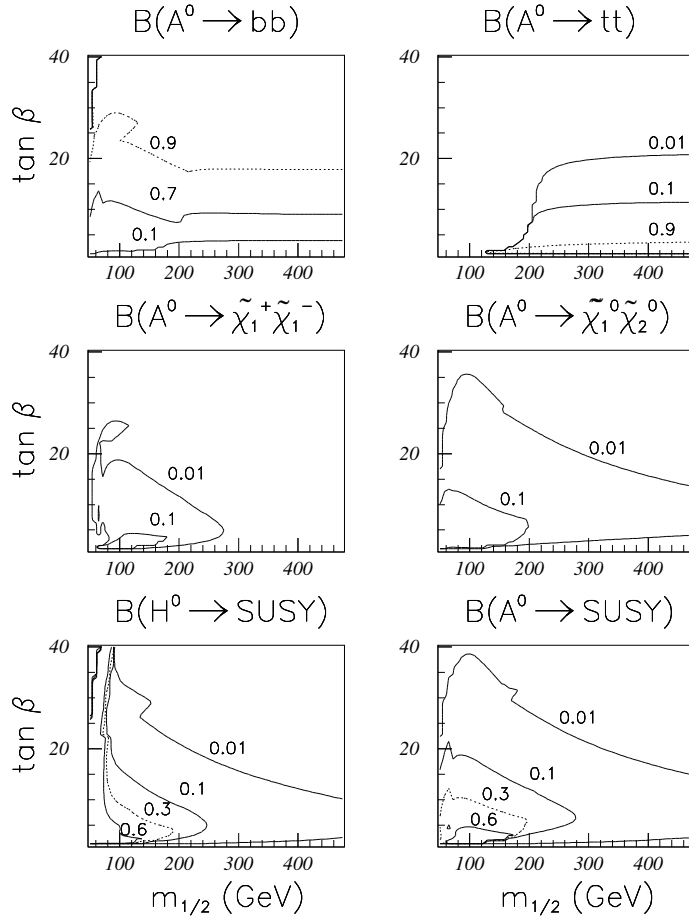


Figure 4: b) We show contours within the  $(m_{1/2}, \tan \beta)$  parameter space of constant branching fraction for the  $A^0 \rightarrow b\bar{b}, t\bar{t}, e_1^+ e_1^-$ , and  $e_1^0 e_2^0$  decay channels, as well as for  $H^0 \rightarrow \text{SUSY}$  and  $A^0 \rightarrow \text{SUSY}$ , summed over all SUSY channels. Results are for the D scenario.

# Dilaton ( $\mu=-$ ) Branching Ratio Contours

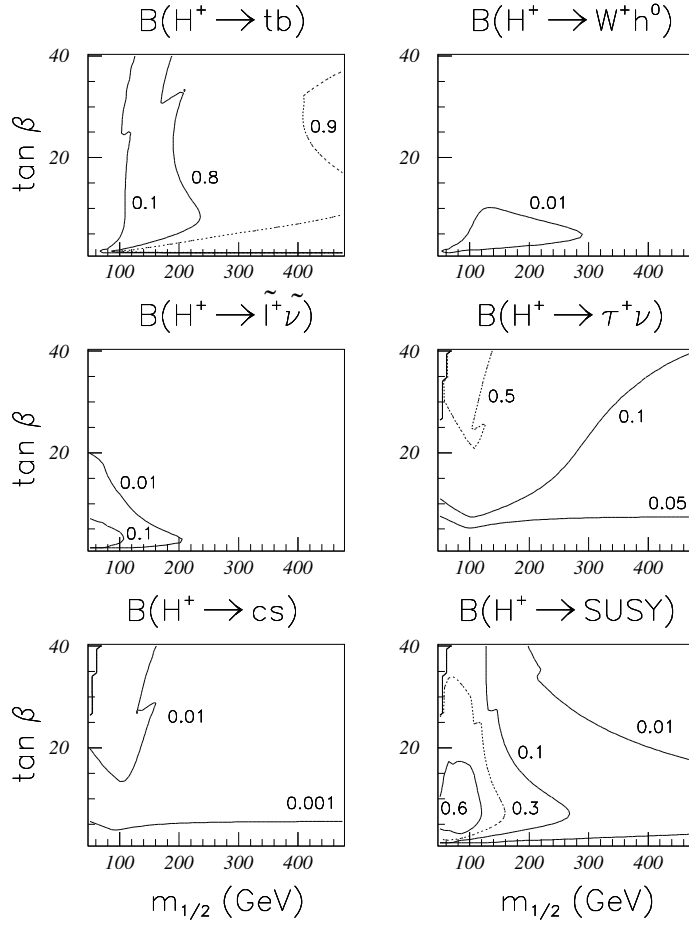


Figure 4: c) We show contours within the  $(m_{1/2}, \tan \beta)$  parameter space of constant branching fraction for the  $H^+ \rightarrow tb, W^+ h^0, \tau^+ \nu, \tilde{l}^+ \tilde{\nu}, c\bar{s}$ , and SUSY, summed over all SUSY channels. Results are for the D scenario.

branching fraction for the  $A^0$  is very tiny.) The  $A^0 \rightarrow Zh^0$  branching fraction is small, but, as we shall see, measurable in some regions of parameter space. For the  $H^\pm$  we display branching fraction contours for  $t\bar{b}$ ,  $W^\pm h^0$ ,  $\tau_\mu e^\pm$ ,  $\mu^\pm$ ,  $\bar{c}s$ , and the sum over all SUSY decays.  $B(A^0 \rightarrow Zh^0)$  is similar to  $B(H^\pm \rightarrow W^\pm h^0)$ .] Several important features of these plots deserve emphasis.

For the  $H^0$  and  $A^0$ , the net branching fraction for SUSY decays declines rapidly with increasing  $\tan\beta$  due to the enhancement of the  $b\bar{b}$  coupling and, hence, increasing relative importance of  $b\bar{b}$  decays.

SUSY decays of the  $H^0$  and  $A^0$  are also small when  $m_{H^0}; m_{A^0} > 2m_t$ , with the relative branching fraction  $B(\text{SUSY})/B(t\bar{t})$  saturating to a constant value below 0.1 for large  $m_{A^0}$  (equivalently large  $m_{1=2}$ ) at fixed  $\tan\beta$ .

For  $m_{H^0}; m_{A^0} > 2m_t$ , the ratio of  $b\bar{b}$  to  $t\bar{t}$  branching fractions rises very rapidly as  $\tan\beta$  increases.

The SUSY decay branching fraction of the  $H^\pm$  is relatively independent of  $\tan\beta$  for lower  $m_{1=2}$  values.

$B(H^\pm \rightarrow W^\pm h^0)$  [as well as  $B(A^0 \rightarrow Zh^0)$ ] is only significant when  $\tan\beta$  and  $m_{1=2}$  are both small.

$B(H^0 \rightarrow h^0 h^0)$  is significant for a larger range of modest  $\tan\beta$  and  $m_{1=2}$  values than the former two branching fractions.

$B(H^\pm \rightarrow \tau^\pm \mu)$  remains significant ( $> 0.1$ ) for a range of  $\tan\beta$  values that becomes increasingly large as  $m_{1=2}$  increases.

These figures show that a measurement of several ratios of branching fractions (e.g.  $\text{SUSY}/b\bar{b}$  for the  $H^0; A^0$  and  $\text{SUSY}/t\bar{t}$  for the  $H^\pm$ ) would determine the values of  $\tan\beta$  and  $m_{1=2}$ . Branching ratios in the other five scenarios display a more or less similar pattern to that found in the D case, although the numerical values at any given  $(m_{1=2}; \tan\beta)$  location can differ substantially. For any given GUT scenario, definite predictions for all other experimental observables are then possible and could be checked for consistency with observations. In particular, the predicted Higgs, neutralino, and chargino masses should agree with the measured values if the GUT scenario is the correct one.

### 3 Discovering the $H^0$ , $A^0$ and $H^\pm$

In this section, we determine the luminosity required in order that discovery of  $H^0 A^0$  and  $H^\pm H^\pm$  be guaranteed over essentially all of the allowed parameter space of the three scenarios. For the models considered in this paper, we find that discovery is always easiest by employing final states in which neither of the Higgs

bosons of the pair decays to a final state containing SUSY particles. The final state configurations we employ for discovery are listed below, along with techniques for isolating them from backgrounds.

I)  $H^0 A^0 \rightarrow 4b$ : We demand observation of four jets which separate into two nearly equal mass two-jet pairs. Event rates for this mode [labelled by N (4b)] include a factor of  $B(H^0 \rightarrow b\bar{b})B(A^0 \rightarrow b\bar{b})$ .

II)  $H^0 A^0$  with  $H^0 \rightarrow h^0 h^0 \rightarrow 4b$  and  $A^0 \rightarrow X$ : it would be sufficient to observe the two  $h^0$ 's by demanding two jet pairs that reconstruct to the known  $m_{h^0}$  recoiling against a reconstructed (from incoming energy and net  $h^0 h^0$  pair four momentum) missing mass that is the same as the  $h^0 h^0$  pair mass. Event rates for this mode [labelled by N (hh)] include a factor of  $B(H^0 \rightarrow h^0 h^0) [B(h^0 \rightarrow b\bar{b})]^2$ .

III)  $H^0 A^0 \rightarrow 4t$ : We can simply demand 10 visible (and moderately energetic/separated) leptons/jets. The predicted rate for such states on the basis of QCD (including 4t production) is quite small. Because of inefficiencies associated with combinatorics, we would not require direct reconstruction of the W's or t's (implying that we would also not be able to require roughly equal Higgs boson masses). Event rates for this mode [labelled by N (4t)] include the effective branching ratio for  $H^0 A^0 \rightarrow 10$  visible leptons/jets, given by  $B(H^0 \rightarrow t\bar{t})B(A^0 \rightarrow t\bar{t})B(t\bar{t} \rightarrow 10 \text{ visible})$ .

IV)  $H^+ H^- \rightarrow 2t2b$ : We insist on 8 jets or 1 lepton plus 6 jets (in particular, fewer than 10 visible leptons/jets so as to discriminate from the above 4t final states) and possibly require that one W and the associated t be reconstructed. Event rates for this mode [labelled by N (tb)] include a factor of  $[B(H^+ \rightarrow t\bar{b})]^2 f 2B(t \rightarrow 2jb)B(t \rightarrow \nu^+ b) + [B(t \rightarrow 2jb)]^2 g$ .

There will also be an overall efficiency factor for detector coverage and for experimentally isolating and detecting these modes. This will be incorporated in our yearly event rate estimates by reducing the total luminosity available (presumed to be  $L = 200 \text{ fb}^{-1}$  per year at  $\sqrt{s} = 1 \text{ TeV}$  and  $L = 1000 \text{ fb}^{-1}$  per year at  $\sqrt{s} = 4 \text{ TeV}$ ) by an overall efficiency factor of 40% (to  $L_e = 80 \text{ fb}^{-1}$  and  $L_e = 400 \text{ fb}^{-1}$ , respectively). We have not performed a detailed simulation, but believe that that such an efficiency is not unreasonable given the fact that backgrounds are relatively small for the above outlined signatures. In particular, since all the final states contain at least four b jets, we can require one or two b-tags (in order to eliminate any residual QCD background) without incurring significant penalty, given that the vertex-tagger should have efficiency of 60% or better for any single b-jet within its acceptance. (Tagging of b-jets would be desirable for cleanly separating  $H^0 A^0$  from  $H^+ H^-$  final states. In the absence of any b-tagging there would be a small number of  $H^+ H^- \rightarrow 4j$  (with  $j = c, s$ ) events that would combine with the  $H^0 A^0 \rightarrow 4b$  final states to the extent that  $m_{H^+} + m_{H^0} = m_{A^0}$ .)

After including branching fractions and the 40% efficiency, something like 20 events should be adequate for detection. In our graphs, we will display 20, 50 and 200 event contours.

If the  $H^0 A^0 \rightarrow 4t$  mode is dominant, we will wish to reconstruct the mass of either the  $A^0$  or the  $H^0$  from the  $4j2b$  decay mode of one of the  $t\bar{t}$  pairs. This will be important both as a means for measuring the mass and also as a means for triggering on  $H^0 A^0$  pair production using just one of the two members of the pair (see Section 4). There will be a further efficiency factor (on top of the above overall efficiency factor) for isolating the relevant events and then reconstructing the mass of the  $A^0$  or  $H^0$ . We estimate this additional efficiency factor to be of order 25% each for the  $A^0$  and  $H^0$ . This is the result that would be obtained from  $[B(t \rightarrow 2jb)]^2$ , with  $\epsilon = 0.55$  for combinatoric and other problems. The low net efficiency ( $0.2 \times 2 \times 0.25 \times 0.4$ ) for events in which either  $m_{H^0}$  or  $m_{A^0}$  could be fully reconstructed implies that an accurate determination of  $m_{H^0} - m_{A^0}$  would require several years of running if  $H^0 A^0 \rightarrow 4t$  is the dominant final state.

There are several reasons why non-SUSY final states are best for discovery:

As illustrated in Figs. 4a-c, branching fractions for SM decays, e.g.  $A^0 \rightarrow b\bar{b}$  or  $t\bar{t}$  and  $H^+ \rightarrow t\bar{b}$ , do not fall much below 0.1;

Unlike the  $b\bar{b}$  channel, mass reconstruction in SUSY modes is not possible (due to missing energy).

Particle multiplicities in the  $4t$  and  $2t2b$  final states are sufficiently large to be very distinctive and free of background, unlike many of the final states associated with SUSY decays.

In Figures 5, 6, and 7 (for the NS, D and HS scenarios, respectively) we give the 20, 50 and 200 event contours in the  $(m_{1=2}; \tan \beta)$  parameter plane for  $H^0 A^0$  discovery modes I, II and III and  $H^+ H^-$  discovery mode IV at  $\sqrt{s} = 1 \text{ TeV}$ . We assume  $L = 200 \text{ fb}^{-1}$  and  $\epsilon = 40\%$  efficiency, i.e.  $L_e = 80 \text{ fb}^{-1}$ . Results are displayed for both signs of  $\mu$ . Also shown are the boundaries defined by the kinematically accessible  $m_{H^0} + m_{A^0} \leq \sqrt{s}$  or  $2m_H \leq \sqrt{s}$  portion of the allowed parameter space (bold solid lines). In comparing scenarios, it will be important to note that the NS scenario plots have greatly expanded axis scales relative to plots for the D and HS scenarios.

As noted earlier, 20 events is likely to be adequate for discovery; the 50 event contour at  $L_e = 80 \text{ fb}^{-1}$  would probably allow discovery at  $L_e = 32 \text{ fb}^{-1}$  and the 200 event contour would allow discovery at  $L_e = 8 \text{ fb}^{-1}$ . These figures show that for all three GUT scenarios at least 20  $H^0 A^0$  events are present in one or more of the modes I-III throughout almost the entire kinematically accessible portion of the allowed  $(m_{1=2}; \tan \beta)$  parameter space. If the 50 event contours are appropriate (because  $L_e$  is a factor of 2.5 smaller) then one begins to see some, but not enormous, sections of parameter space such that  $H^0 A^0$  detection would not be

possible. If efficiencies and integrated luminosity were in combination a factor of 10 worse than anticipated, the 200 event contours might apply; they indicate that  $H^0 A^0$  detection would then be possible only in the part parameter space characterized by small values of  $m_{1=2}$  and large values of  $\tan \beta$ .

In these same figures, the 20, 50 and 200 event contours for the  $H^+ H^-$  discovery mode IV show that 20 events are found for all of the constraint and kinematically allowed parameter space except a small wedge at small  $m_{1=2}$  values. The 200 event contours (equivalent to 20 events at  $L_e = 5 \text{ fb}^{-1}$ ) cover nearly as a large section of parameter space. Thus, even if efficiency and luminosity are in combination a factor of 10 worse than anticipated,  $H^+ H^-$  discovery after just one year of running would be possible over the bulk of parameter space. The somewhat better guarantees for the  $H^+ H^-$  mode as compared to the  $H^0 A^0$  mode derive simply from the larger  $H^+ H^-$  cross section which is roughly a factor of 3 larger than that for  $H^0 A^0$ .

This same analysis can be repeated for 4 TeV and  $L = 1000 \text{ fb}^{-1}$  (implying  $L = 400 \text{ fb}^{-1}$  for  $\epsilon = 0.4$  efficiency) with very similar results. The kinematic range is much greater, allowing  $H^0 A^0$  and  $H^+ H^-$  production out to masses  $m_{A^0} = m_{H^0} = m_H < 2 \text{ TeV}$ . (The limited NS parameter space implies that such energies are not needed were this the correct GUT scenario). If 20 events are adequate (and they would certainly be rather spectacular events at high Higgs boson mass) then both  $H^0 A^0$  and  $H^+ H^-$  detection would be possible for nearly all of the constraint/kinematically allowed parameter space for all three GUT scenarios. Diminution in coverage due to poorer efficiency or lower luminosity follows much the same pattern as described for the  $\sqrt{s} = 1 \text{ TeV}$ ,  $L = 200 \text{ fb}^{-1}$  case. To illustrate, we present the 20, 50 and 200 event contours for  $H^0 A^0$  (neutral states I-III) and  $H^+ H^-$  (neutral state IV) in the D scenario, Fig. 8.

## 4 Measuring Ratios of Branching Fractions and Discriminating Between Models

In this section we discuss the prospects for measuring the relative size of the various branching fractions for different decay modes of a given Higgs boson and for using such measurements to pin down the GUT model and parameter choices within a given GUT model. Additional information is contained in the absolute rates for different types of neutral states. However, it is likely that greater uncertainty will be associated with absolute rates than with ratios of rates, since some types of efficiencies will cancel out of the ratios.

The key to determining the relative magnitude of the branching fractions for different neutral state decays is to first identify and mass-reconstruct ('tag') one of the Higgs bosons in the  $H^0 A^0$  or  $H^+ H^-$  pair neutral state, and then compare the relative rates for different types of decays of the second Higgs boson. Identification and mass-reconstruction of the first Higgs boson requires using one of its fully reconstructable neutral states. As additional verification that the event corresponds

## No Scale Scenario Discovery Contours

$$E_{cm}=1 \text{ TeV}, L_{eff}=80 \text{ fb}^{-1}$$

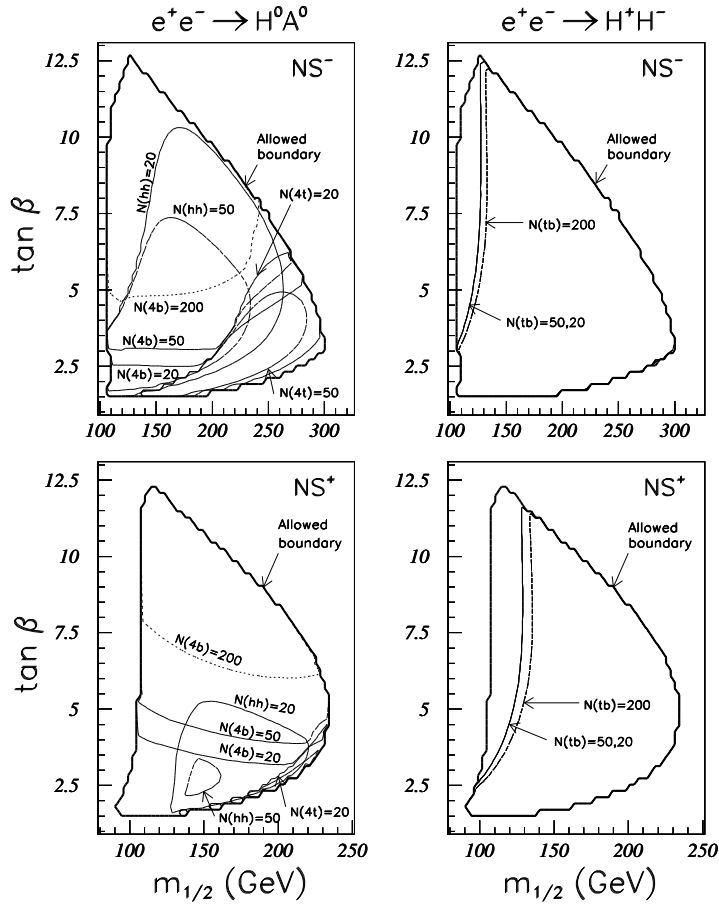


Figure 5: We show  $NS$  model 20, 50 and 200 event contours within the kinematically accessible portion of the allowed  $(m_{1/2}; \tan \beta)$  parameter space for  $H^0 A^0$  discovery modes I, II, III and  $H^+ H^-$  discovery mode IV, assuming  $L_e = 80 \text{ fb}^{-1}$ .

## Dilaton Scenario Discovery Contours

$$E_{cm}=1 \text{ TeV}, L_{eff}=80 \text{ fb}^{-1}$$

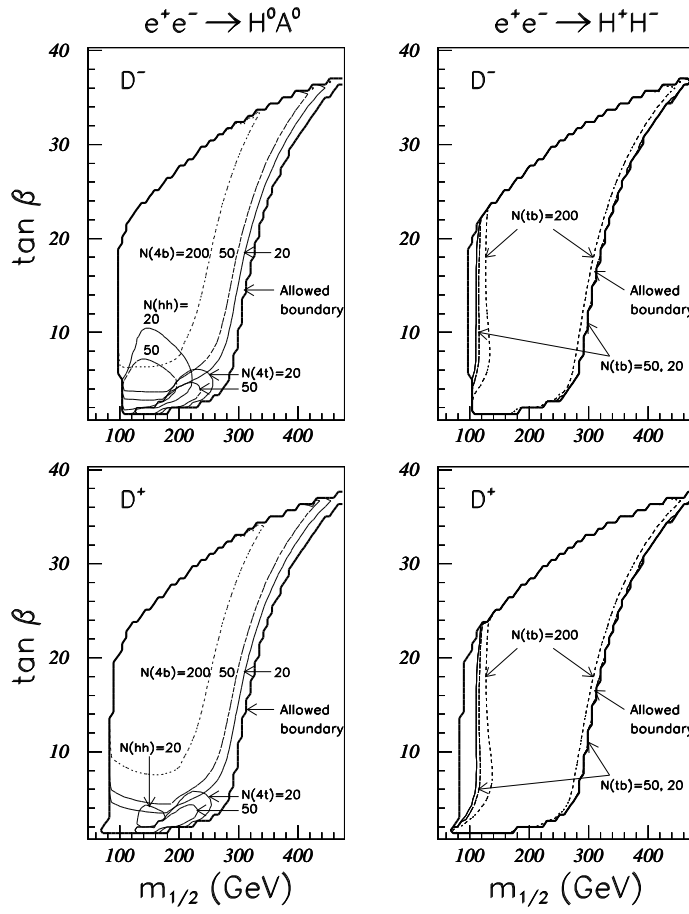


Figure 6: We show  $D^-$  model 20, 50 and 200 event contours within the kinematically accessible portion of the allowed  $(m_{1/2}; \tan \beta)$  parameter space for  $H^0 A^0$  discovery modes I, II, III and  $H^+ H^-$  discovery mode IV, assuming  $L_e = 80 \text{ fb}^{-1}$ .

## Heavy Scalar Scenario Discovery Contours

$$E_{cm}=1 \text{ TeV}, L_{eff}=80 \text{ fb}^{-1}$$

$$e^+e^- \rightarrow H^0 A^0$$

$$e^+e^- \rightarrow H^+ H^-$$

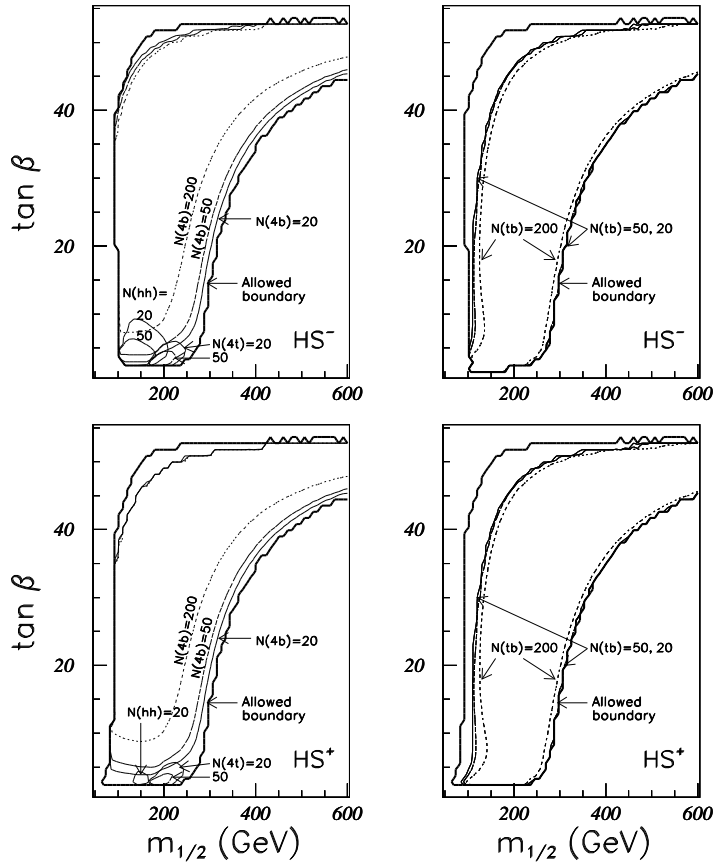


Figure 7: We show  $HS$  model 20, 50 and 200 event contours within the kinematically accessible portion of the allowed  $(m_{1/2}; \tan \beta)$  parameter space for  $H^0 A^0$  discovery modes I, II, III and  $H^+ H^-$  discovery mode IV, assuming  $L_e = 80 \text{ fb}^{-1}$ .

## Dilaton Scenario Discovery Contours

$$E_{cm}=4 \text{ TeV}, L_{eff}=400 \text{ fb}^{-1}$$

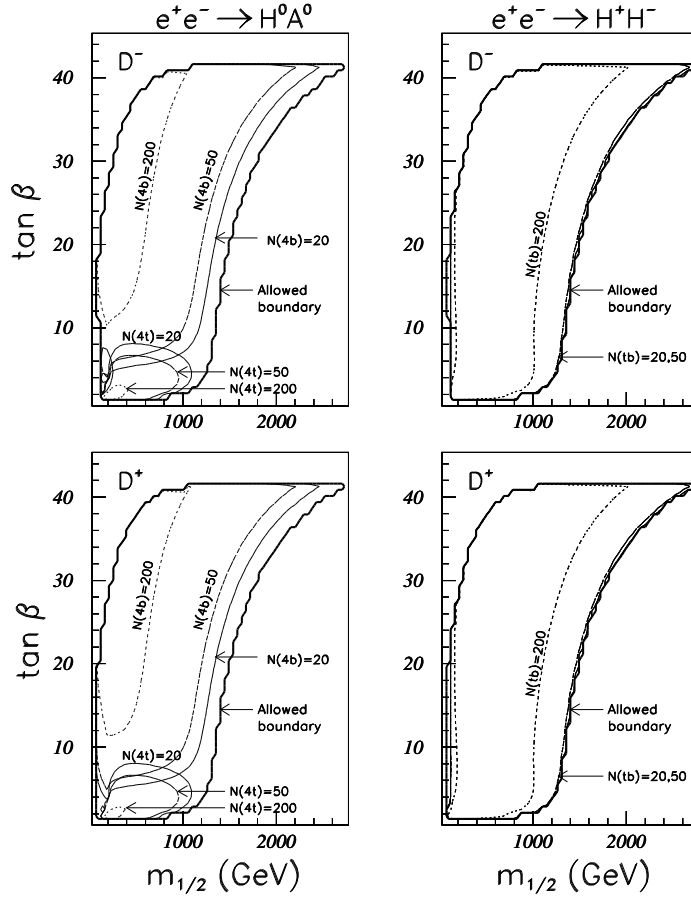


Figure 8: We show  $D^-$  model 20, 50 and 200 event contours within the kinematically accessible portion of the allowed  $(m_{1/2}; \tan \beta)$  parameter space for  $H^0 A^0$  discovery modes I, II, III and  $H^+ H^-$  discovery mode IV, assuming  $L_e = 400 \text{ fb}^{-1}$  at  $\sqrt{s} = 4 \text{ TeV}$ .

to Higgs pair production, we would require that the missing mass (as computed using the incoming center-of-mass four-momentum and the four-momentum of the reconstructed Higgs) be roughly equal to the mass of the identified Higgs. For identification and mass-reconstruction of the first Higgs boson, we employ:

$$H^0 A^0 \text{ with } H^0 \rightarrow 2b \text{ or } A^0 \rightarrow 2b;$$

$$H^0 A^0 \text{ with } H^0 \rightarrow 2t \text{ or } A^0 \rightarrow 2t \mid \text{note that, unlike the } 4t \text{ discovery channel, reconstruction of the } 2t \text{ mass will be necessary, and will be accompanied by an extra efficiency penalty relative to } H^0 \rightarrow 2b \text{ or } A^0 \rightarrow 2b \text{ tagging of } \epsilon_{t \rightarrow b\bar{b}}^{\text{tag}} [B(t \rightarrow 2j\bar{b})]^2 \approx 0.25 \text{ (for } \epsilon = 0.55), \text{ as discussed earlier;}^3$$

$$H^0 A^0 \text{ with } H^0 \rightarrow h^0 h^0 \rightarrow 4b;$$

$$H^+ H^- \text{ with } H^+ \rightarrow t\bar{b} \text{ or } W^- 2b \rightarrow 2j2b; \text{ or the reverse } \mid \text{ } t\bar{b} \text{ mass reconstruction will be necessary.}$$

In the case of  $H^0 A^0$  pair production, in determining that the second (non-tagged) member of the pair decays to  $t\bar{t}$ , we will again demand full  $t\bar{t}$  reconstruction, and we will apply the extra  $\epsilon_{t \rightarrow b\bar{b}}$  efficiency penalty relative to  $b\bar{b}$  decay. This might be somewhat too conservative an approach, but does simplify our analysis since the event rates of interest involving  $t\bar{t} + b\bar{b}$  decays will then be proportional to the effective branching fractions

$$B_e(H^0; A^0 \rightarrow b\bar{b} + t\bar{t}) = B(H^0; A^0 \rightarrow b\bar{b}) + \epsilon_{t \rightarrow b\bar{b}} B(H^0; A^0 \rightarrow t\bar{t}) : \quad (1)$$

Because  $m_{A^0} \approx m_{H^0}$  over much of parameter space, we will presume that it is not possible to separate the  $A^0$  and  $H^0$  from one another. We also stick to our simplifying assumption that the overall efficiency,  $\epsilon$ , associated with detector coverage, b-tagging and so forth does not depend upon the final state, except that in the case of  $t\bar{t}$  decay we include an extra  $\epsilon$  in  $\epsilon_{t \rightarrow b\bar{b}}$ , as discussed above and as incorporated through  $B_e$  defined in Eq. (1). With these assumptions, the following ratios of branching fractions can be extracted directly from experimental observations using the measured values of  $B(h^0 \rightarrow b\bar{b})$  and  $B(t \rightarrow 2j\bar{b})$ .

$$\frac{B(H^0 \rightarrow \text{SUSY}) B_e(A^0 \rightarrow b\bar{b} + t\bar{t}) + B(A^0 \rightarrow \text{SUSY}) B_e(H^0 \rightarrow b\bar{b} + t\bar{t})}{B_e(H^0 \rightarrow b\bar{b} + t\bar{t}) B_e(A^0 \rightarrow b\bar{b} + t\bar{t})} \quad (2)$$

$$\frac{B(H^0 \rightarrow t\bar{t}) B(A^0 \rightarrow b\bar{b}) + B(A^0 \rightarrow t\bar{t}) B(H^0 \rightarrow b\bar{b})}{B(H^0 \rightarrow b\bar{b}) B(A^0 \rightarrow b\bar{b})} \quad (3)$$

$$\frac{B(H^0 \rightarrow h^0 h^0) B(A^0 \rightarrow b\bar{b})}{B(H^0 \rightarrow b\bar{b}) B(A^0 \rightarrow b\bar{b})} \quad (4)$$

---

<sup>3</sup>These details for the  $t\bar{t}$  final state are only relevant for  $B_e$  defined in Eq. (1) and the ratios of Eqs. (2) and (3) below, and then only when  $B(H^0; A^0 \rightarrow t\bar{t})$  are relatively large.

$$\frac{B(A^0 \rightarrow Zh^0)B(H^0 \rightarrow b\bar{b})}{B(H^0 \rightarrow b\bar{b})B(A^0 \rightarrow b\bar{b})} \quad (5)$$

$$\frac{B(H^+ \rightarrow \text{SUSY})B(H^- \rightarrow b\bar{t}) + B(H^- \rightarrow \text{SUSY})B(H^+ \rightarrow t\bar{b})}{B(H^+ \rightarrow t\bar{b})B(H^- \rightarrow b\bar{t})} \quad (6)$$

$$\frac{B(H^+ \rightarrow W^+ \gamma)B(H^- \rightarrow b\bar{t}) + B(H^- \rightarrow W^- \gamma)B(H^+ \rightarrow t\bar{b})}{B(H^+ \rightarrow t\bar{b})B(H^- \rightarrow b\bar{t})} \quad (7)$$

$$\frac{B(H^+ \rightarrow h^0 W^+)B(H^- \rightarrow b\bar{t}) + B(H^- \rightarrow h^0 W^-)B(H^+ \rightarrow t\bar{b})}{B(H^+ \rightarrow t\bar{b})B(H^- \rightarrow b\bar{t})} \quad (8)$$

As a shorthand, we will employ the notations

$$\frac{2B(H^0; A^0 \rightarrow \text{SUSY})^+}{B_e(H^0; A^0 \rightarrow b\bar{b}; t\bar{t})}^* ; \quad \frac{2B(H^0; A^0 \rightarrow t\bar{t})^+}{B(H^0; A^0 \rightarrow b\bar{b})}^* ; \quad (9)$$

for the ratios of Eqs. (2) and (3), respectively. The ratios of Eqs. (6)–(8) reduce to

$$\frac{2B(H^+ \rightarrow \text{SUSY}; W^+; h^0)}{B(H^+ \rightarrow t\bar{b})} ; \quad (10)$$

respectively. We retain both  $b\bar{b}$  and  $t\bar{t}$  final states in Eq. (2), using the combination defined in  $B_e$ , in order that we may assess the importance of SUSY decays both in regions where  $b\bar{b}$  decays of the  $H^0; A^0$  are dominant and in regions where  $t\bar{t}$  decays are important.

In estimating the accuracy with which these ratios can be measured experimentally, it is important to keep track of the actual final state in which the observation occurs and the effective efficiency for observing that final state. We make this explicit below.

The event rate for the numerator of Eq. (2) is obtained by multiplying the rate for  $H^0 A^0$  pair production by (the overall efficiency factor) times the indicated sum of branching ratio products:  $[B(H^0 \rightarrow \text{SUSY})B_e(A^0 \rightarrow b\bar{b} + t\bar{t}) + B(A^0 \rightarrow \text{SUSY})B_e(H^0 \rightarrow b\bar{b} + t\bar{t})]$ .

The numerator of Eq. (4) must be measured in the final state in which both  $h^0$ 's decay to  $b\bar{b}$ . Thus, the event rate associated with determining the numerator is obtained by multiplying the  $H^0 A^0$  pair production rate by a factor of  $[B(h^0 \rightarrow b\bar{b})]^2$  times the overall efficiency times  $B(H^0 \rightarrow h^0 h^0)B(A^0 \rightarrow b\bar{b})$ .

The event rate associated with measuring the numerator of Eq. (3) is obtained using a factor of  $\epsilon_{t\bar{t} \rightarrow b\bar{b}} = 4[B(t \rightarrow 2jb)^2]$  times  $B(H^0 \rightarrow t\bar{t})B(A^0 \rightarrow b\bar{b}) + B(A^0 \rightarrow t\bar{t})B(H^0 \rightarrow b\bar{b})$ .

The event rate for the numerator of Eq. (5) is computed using the factor  $B(H^0 \rightarrow b\bar{b})B(A^0 \rightarrow Zh^0)B(H^0 \rightarrow b\bar{b})$ . This implicitly assumes that we can sum over all  $Z$  decays, as would be possible since the  $Z$  mass can be reconstructed from the  $\sqrt{s}$  value and the momenta of the four  $b$ 's.

The event rate for the numerator of Eq. (6) is obtained by multiplying the  $H^+H^-$  event rate by the factor  $B(t \rightarrow 2jb) [B(H^+ \rightarrow \text{SUSY})B(H^- \rightarrow b\bar{b}) + B(H^- \rightarrow \text{SUSY})B(H^+ \rightarrow t\bar{b})]$ .

The event rate for the numerator of Eq. (7) is computed by multiplying the pair rate by  $B(t \rightarrow 2jb) [B(H^+ \rightarrow \tau^+ \nu_\tau)B(H^- \rightarrow b\bar{b}) + B(H^- \rightarrow \tau^- \nu_\tau)B(H^+ \rightarrow t\bar{b})]$ .

The rate for the numerator of Eq. (8) is computed using the factor  $B(h \rightarrow b\bar{b})B(t \rightarrow 2jb) [B(H^+ \rightarrow h^0 W^+)B(H^- \rightarrow b\bar{b}) + B(H^- \rightarrow h^0 W^-)B(H^+ \rightarrow t\bar{b})]$ .

The factors for the denominators are obtained by multiplying the indicated branching ratio product by  $\Gamma$  in the case of the neutral Higgs ratios, and by  $[B(t \rightarrow 2jb)]^2$  in the case of charged Higgs ratios.

When dividing the SUSY collection of final states (as simply identified by missing energy) into subcategories of a certain number of leptons and/or jets, the full set of appropriate branching ratios are included in all the chain decays leading to the specified final state.

As noted, the overall factor of  $\Gamma$  common to all rates is incorporated by reducing the full luminosity to the effective luminosity  $L_e$ . Rates for the standard  $L_e = 80 \text{ fb}^{-1}$  are thus obtained by computing the pair production cross section, multiplying by  $L_e$  and then including all the above factors after removing the overall multiplicative  $\Gamma$  contained in each. The bottom line is that even though we plot the ratios listed, the statistical errors we shall discuss will be based on the actual number of events as obtained according to the above-outlined procedures.

The utility of the above ratios derives from the following general features. The 1st ratio is primarily a function of  $\tan \beta$ . The 2nd provides an almost direct determination of  $\tan \beta$  since  $t\bar{t} \rightarrow b\bar{b}$  is roughly proportional to  $\cot^4 \beta$  in the MSSM. The ratios of Eqs. (6) and (7) both exhibit substantial and rather orthogonal variation as a function of  $\tan \beta$  and  $m_{1=2}$ . The ratio of Eq. (4) is proportional to the relative strength of the  $H^0 \rightarrow h^0 h^0$  trilinear coupling as compared to the  $H^0 \rightarrow b\bar{b}$  coupling. This could be the first direct probe of Higgs trilinear couplings. The ratios of Eqs. (5) and (8) would probe the very interesting Higgs Higgs{vector-boson couplings. These features will be illustrated shortly.

#### 4.1 Resolving Ambiguities in Identifying Different Final States

Since all SUSY final states will contain substantial missing energy, the ambiguities in separating SUSY decays from others are limited. We discuss below the procedures for removing the only ambiguities that appear to be of importance.

(A) A potential ambiguity arises in  $\tilde{\nu}^+ + E_T$  final states of the  $H^+$  to which the SUSY  $\tilde{e}^+ e^-$  and  $e^+ e^-$  decay modes and the SM  $H^+ \rightarrow \tilde{\nu}^+ \nu^0$  decay modes all contribute. The  $H^+ \rightarrow \tilde{\nu}^+ \nu^0$  decay can be identified using kinematic constraints. Consider the c.m. system of the decaying  $H^+$  (as determined using incoming beam information and the tagged  $H^-$  four-momentum). To the extent that  $m_e$  can be neglected and, therefore, the  $\tilde{e}^\pm$  decays collinearly to  $\tilde{\nu}^0$ , all of which move opposite the primary  $\tilde{\nu}^+$ , one must have  $E = \sqrt{E_T^2 + m_e^2}$  where  $E$  is the energy of the observed  $\tilde{\nu}^0$ . SUSY events of any type will normally violate this constraint. In what follows, the  $\tilde{e}^+ e^-$  and  $e^+ e^-$  decays are both included in the overall SUSY decay rate of the  $H^+$ .

(B) In  $H^0$  or  $A^0$  decay,  $\tilde{\nu}^0$  decays contribute to the same  $\tilde{\nu}^+ \tilde{\nu}^- + E_T$  final states to which the SUSY modes  $\tilde{e}^+ \tilde{e}^-$  and  $e^+ e^-$  contribute. The procedure for eliminating the  $\tilde{\nu}^0$  decay is analogous to that discussed in (A) for removing  $H^+ \rightarrow \tilde{\nu}^+ \nu^0$  decays. We again note that, for most events, the  $m_e$  mass can be neglected relative to its momentum. In the (known) rest frame of the Higgs, the collinear approximation implies that the  $\tilde{\nu}^+$  and  $\tilde{\nu}^-$  and their associated neutrinos travel in essentially the same directions as the parent  $\tilde{\nu}^+$  and  $\tilde{\nu}^-$ , respectively. As a result, such events must have  $\sqrt{E_+^2 + E_-^2} = \sqrt{E_T^2 + m_e^2}$  where  $E_\pm$  are the observed energies of the  $\tilde{\nu}^\pm$  in the Higgs rest frame. The very non-collinear SUSY modes would generally be far from approximately satisfying this constraint. Kinematic constraints do not allow an event-by-event separation of the two SUSY modes,  $\tilde{e}^+ \tilde{e}^-$  and  $e^+ e^-$ , in the  $\tilde{\nu}^+ \tilde{\nu}^- + E_T$  final state. These are lumped together as part of the overall SUSY decay branching fraction.

(C) Events in which the unreconstructed Higgs boson/decay is  $H^0$  or  $A^0 \rightarrow \tilde{t}\bar{t}$ ,  $\tilde{\nu}^0 2j2b$  or  $H^\pm \rightarrow \tilde{t}b \rightarrow \tilde{\nu}^0 b\bar{b}$  can be eliminated by using the incoming beam energy/momentum 4-vector, subtracting the momenta of all visible final state leptons and jets, and computing the invariant mass of the resulting difference 4-vector. This would belong to the  $\tilde{\nu}^0$  in the above cases. A cut requiring a substantial value would eliminate the above final states and be highly efficient in retaining true SUSY decays. For parameters such that the rates for single neutrino events (as defined by the above procedure and requiring a small value for the difference 4-vector mass) are significant, we shall find that the  $H^0/A^0 \rightarrow \tilde{t}\bar{t}$  and  $H^\pm \rightarrow \tilde{t}b$  branching fractions can be directly measured with reasonable accuracy (using all-jet modes). The predicted single neutrino rate could then be compared to that observed as a further check. Events where the unreconstructed Higgs/decay is  $H^0$  or  $A^0 \rightarrow \tilde{t}\bar{t} \rightarrow 2\tilde{\nu}^0 2b$  cannot be eliminated by the above technique. However, the branching fractions,  $B(H^0/A^0 \rightarrow \tilde{t}\bar{t})$ , measured in all-jet final states can be employed to make an appropriate correction. The single neutrino rates, as defined above, may allow a double-check of the all-jet final state determinations of the  $\tilde{t}\bar{t}$  branching fractions.

(D) Other ambiguities include events in which the second Higgs boson/decay is:  $A^0 \rightarrow Z h^0 \rightarrow Z^+ Z^-$ , where the  $Z$  decays invisibly or to  $\tilde{\nu}^+ \tilde{\nu}^-$ ;  $H^\pm \rightarrow W^\pm h^0$ !

$W^+ \rightarrow \nu_e e^+$  where the  $W$  decays leptonically; and  $H^0 \rightarrow h^0 h^0 \rightarrow \nu_e \nu_e e^+ e^+$ . The common characteristic of all these is the presence of missing energy from  $\nu_e$ ,  $W$  and/or  $Z$  decays that is due to more than a single neutrino and that makes it impossible to either directly or indirectly reconstruct the mass of the  $h^0$ ,  $W$  and/or  $Z$ . However, the event rates for these processes are so low that they can be included in SUSY decays without any visible alteration of the effective SUSY branching fraction. Further, whenever the  $H^0 \rightarrow h^0 h^0$ ,  $A^0 \rightarrow Z h^0$  or  $H^\pm \rightarrow W^\pm h^0$  decays are significant, we shall see that at least a rough measurement of the corresponding branching ratio will be possible in all-jet modes. Given the known  $Z \rightarrow \nu_e \bar{\nu}_e$  and  $h^0 \rightarrow \nu_e \bar{\nu}_e$  branching fractions, a correction could then be made using a Monte Carlo simulation.

## 4.2 Ratio Contours, Error Estimates and Model Discrimination

In order to determine how well we can measure the ratios of Eqs. (2), (3), (4), (5), (6), (7), and (8), we have proceeded as follows. For each of the six scenarios ( $D$ ,  $D^+$ , ...) and for a given  $(m_{1=2}; \tan \beta)$  choice within the allowed parameter space of a given scenario, we first compute the expected number of events available for determining the numerator or denominator of each ratio. The ingredients (such as branching ratios and efficiencies) in the event number computations for each channel were given earlier. The expected number of events in the numerator or denominator is taken as the mean value in determining a Poisson distribution for that event number; if the mean number of events is  $\geq 30$ , then we use a Gaussian approximation to the distribution. From the event number distributions we compute the probability for the numerator and denominator of each ratio to take on given values. (We fluctuate the event numbers and then correct for branching fractions and efficiencies.) The probability of the resulting value for the ratio is then simply the product of these probabilities. The probabilities for different combinations that yield the same value for the ratio are summed. In this way, we obtain a probability for every possible value of the ratio. These probabilities are re-ordered so as to form a distribution. The lower (upper) limit for the ratio at this  $(m_{1=2}; \tan \beta)$  value is then found by adding up the probabilities, starting from zero, until the sum of is 15.9% (84.1%). In other words, the confidence level that the true value of the ratio is higher (lower) than the lower (upper) limit is 84.1%. These would be the 1 upper/lower limits for the ratio in the limit where the distribution of the ratio is normal.

In computing the number of events available for determining the numerator or denominator (or one of the independent contributions thereto) we include only fully reconstructable final states for the tagged Higgs boson. The branching ratios and efficiency factors were detailed below Eq. (10). We presume  $L_e = 80 \text{ fb}^{-1}$  at 1 TeV ( $L_e = 400 \text{ fb}^{-1}$  at 4 TeV). The efficiency factor,  $\epsilon$ , included in  $L_e$  should

reflect efficiencies associated with identifying a particular type of event in such a way as to eliminate backgrounds, e.g. via b-tagging, cuts on  $E_T$ , and so forth; the appropriate to the current situation where one of the Higgs must be clearly 'tagged' (as defined earlier) will probably be smaller than that appropriate to simply discovering a signal, given the need to clearly separate different types of final states from one another. Thus, the above  $L_e = 80 \text{ fb}^{-1}$  ( $400 \text{ fb}^{-1}$ ) values probably would only be achieved after several years of running. We re-emphasize that an implicit approximation to our approach is that  $L_e$  is the same for all the observationally/statistically independent final states that appear in the numerator and denominator of a given ratio. [Aside from our special  $\hat{= 0.55}$  correction for  $t\bar{t}$  reconstruction, the only explicitly channel-dependent factors that have been included are the relevant branching fractions, as detailed below Eq. (10).] Presumably, this will not be true in practice, but it is at least a reasonable first approximation. Full detector specification and simulation would be necessary to do better.

In Figs. 9, 10, 11, 12, 13, 14, and 15 we plot contours of constant values for the ratios of Eqs. (2), (3), (4), (5), (6), (7), and (8) within the  $\sqrt{s} = 1 \text{ TeV}$  constraint/kinematically allowed  $(m_{1=2}; \tan \beta)$  parameter space. Associated with each such contour, we give two additional contours showing how much the  $\tan \beta$  value at a given (known) value of  $m_{1=2}$  would have to change in order to reproduce the values obtained for deviations in the ratio at the  $1\sigma$  statistical level. [As previously explained,  $1\sigma$  is our shorthand phrase for deviations such that the ratio has 84.1% probability of being lower (higher) than the upper (lower) limit.] We do not consider errors when there are fewer than 4 events that can be used to determine the numerator for one of these ratios. The 4-event contours are indicated on the figures.

Consider first the relative SUSY branching ratio contours of Eqs. (2) and (6) displayed in Figs. 9 and 13, respectively. For most points in parameter space, a simultaneous measurement of the two ratios will determine a fairly small and unique region in the parameter space of a given model that is simultaneously consistent with both measurements at the  $1\sigma$  level.

If  $\tan \beta$  is not large, then measuring  $B(H^+ \rightarrow t^+ \bar{b}) = B(H^+ \rightarrow t^+ \bar{b})$  via the ratio of Eq. (7) can provide a second determination of  $\tan \beta$ . The dependence of this ratio on  $\tan \beta$  for a selection of  $m_{H^+}$  values is illustrated in Fig. 16. There, the ratio is computed at tree level. We see that the ratio depends sensitively on  $\tan \beta$  at fixed  $m_{H^+}$  for  $\tan \beta < 6$ . For such  $\tan \beta$  values, measurement of the ratio provides an excellent  $\tan \beta$  determination. However, when  $\tan \beta$  is large the  $t^+ \bar{b}$  ratio becomes independent of  $\tan \beta$  and sensitivity is lost. Note also that the ratio becomes independent of  $m_{H^+}$  when  $m_{H^+}$  is large. Thus, when both  $m_{H^+}$  and  $\tan \beta$  are large, this ratio will provide little information regarding location in parameter space.

Contours of constant  $B(H^+ \rightarrow t^+ \bar{b}) = B(H^+ \rightarrow t^+ \bar{b})$  in  $(m_{1=2}; \tan \beta)$  parameter space are displayed in Fig. 14. It is also useful to plot these same contours in  $(m_{H^+}; \tan \beta)$  parameter space, as done in Fig. 17. In both figures, one observes

$$2\langle B(H^0, A^0 \rightarrow \text{SUSY})/B_{\text{eff}}(H^0, A^0 \rightarrow bb \text{ or } tt) \rangle$$

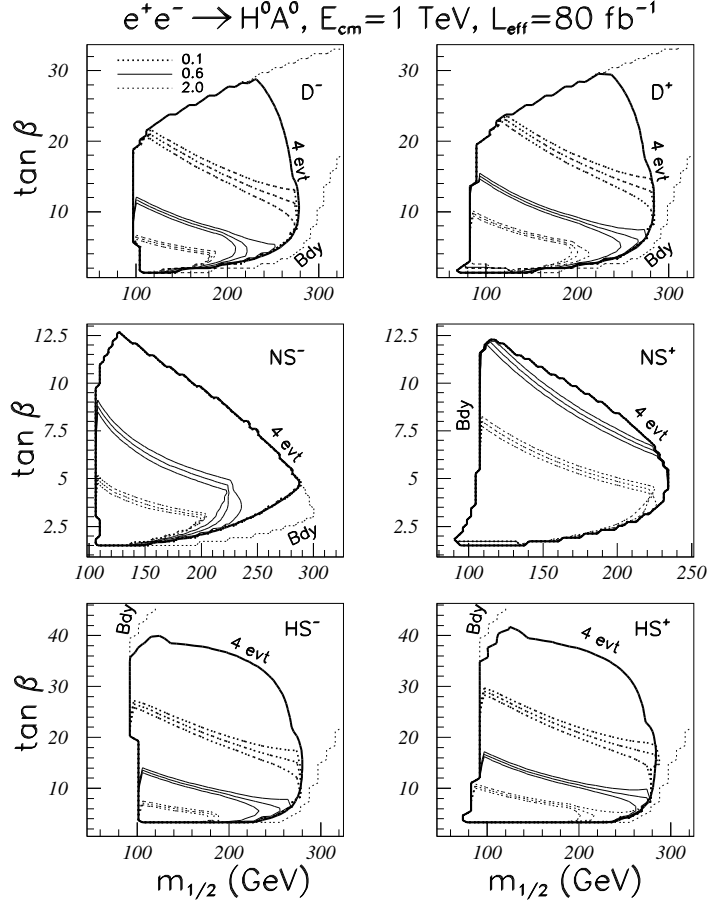


Figure 9: We plot contours, along which the ratio of Eq. (2) has a given constant value, within the constraint/kinematically allowed  $(m_{1/2}; \tan \beta)$  parameter space of the  $D^-$ ,  $D^+$ ,  $NS^-$ ,  $NS^+$ ,  $HS^-$ , and  $HS^+$  models. Results are shown for the same three central values for all models. For each central value, three lines are drawn. The central line is for the central value. The other two lines are contours for which the ratio deviates by  $\pm 1$  statistical error from the central value. Bold lines indicate the boundary beyond which fewer than 4 events are found in the final states used to measure the numerator of the ratio.

$$2\langle B(H^0, A^0 \rightarrow tt)/B(H^0, A^0 \rightarrow bb) \rangle$$

$$e^+e^- \rightarrow H^0 A^0, E_{cm}=1 \text{ TeV}, L_{eff}=80 \text{ fb}^{-1}$$

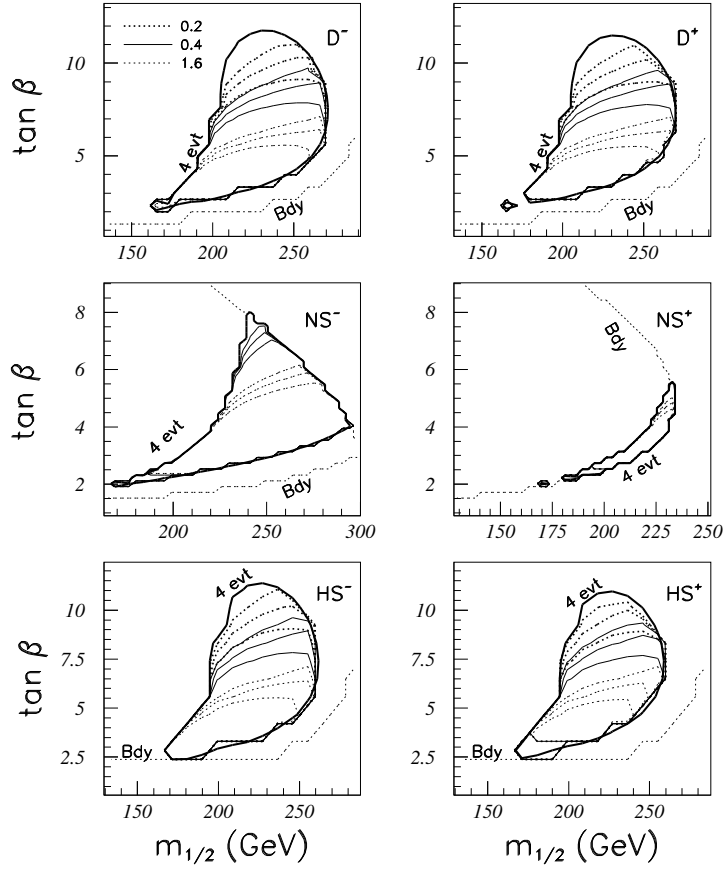


Figure 10: As in Fig. 9, but for the ratio of Eq. (3).

$$B(H^0 \rightarrow h^0 h^0)/B(H^0 \rightarrow b\bar{b})$$

$$e^+e^- \rightarrow H^0 A^0, E_{cm}=1 \text{ TeV}, L_{eff}=80 \text{ fb}^{-1}$$

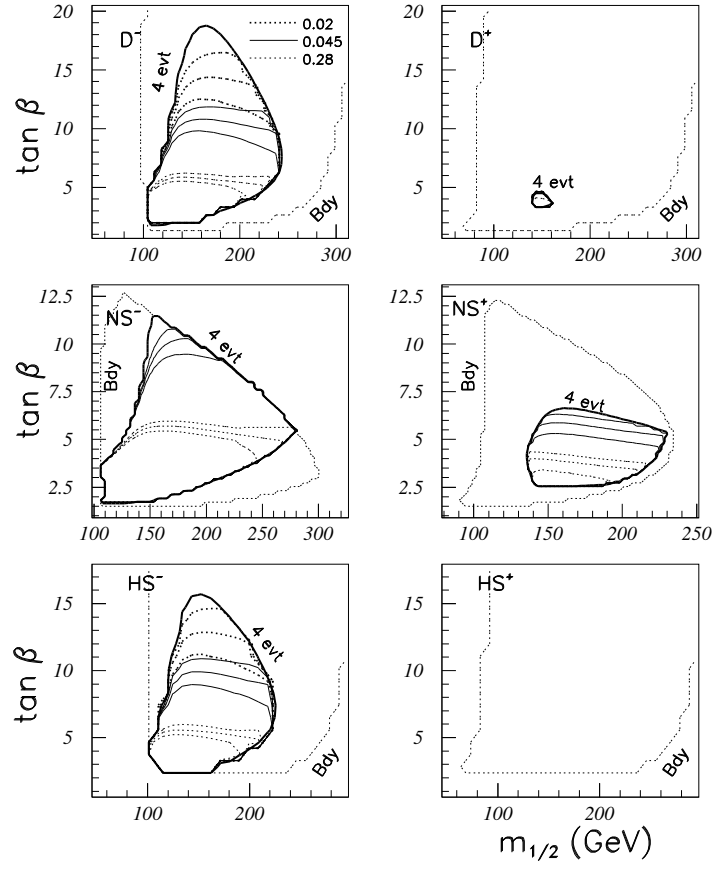


Figure 11: As in Fig. 9, but for the ratio of Eq. (4).

$$B(A^0 \rightarrow Z^0 h^0)/B(A^0 \rightarrow b\bar{b})$$

$$e^+e^- \rightarrow H^0 A^0, E_{cm}=1 \text{ TeV}, L_{eff}=80 \text{ fb}^{-1}$$

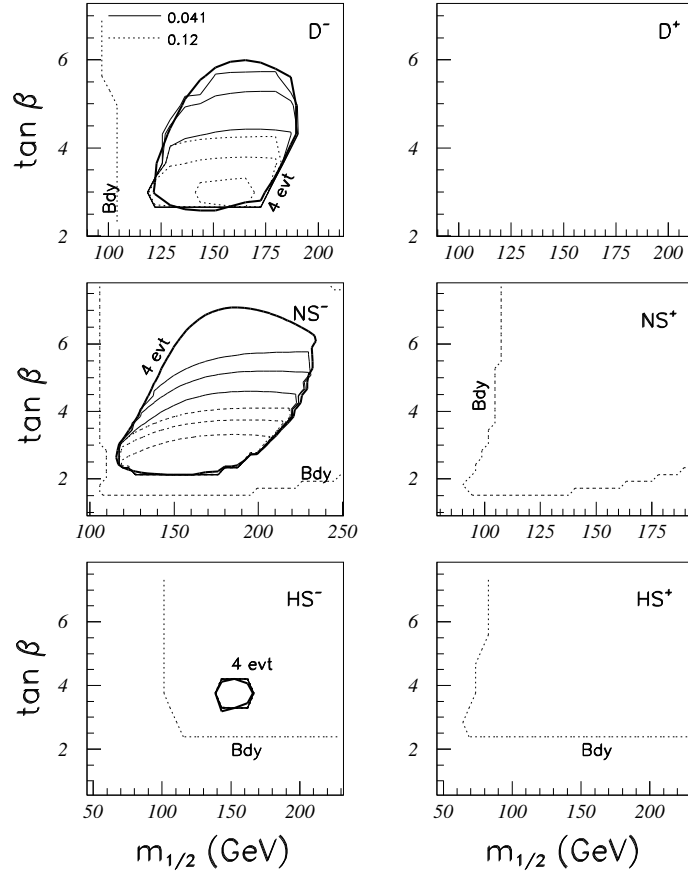


Figure 12: As in Fig. 9, but for the ratio of Eq. (5).

$$2*B(H^+ \rightarrow \text{SUSY})/B(H^+ \rightarrow tb)$$

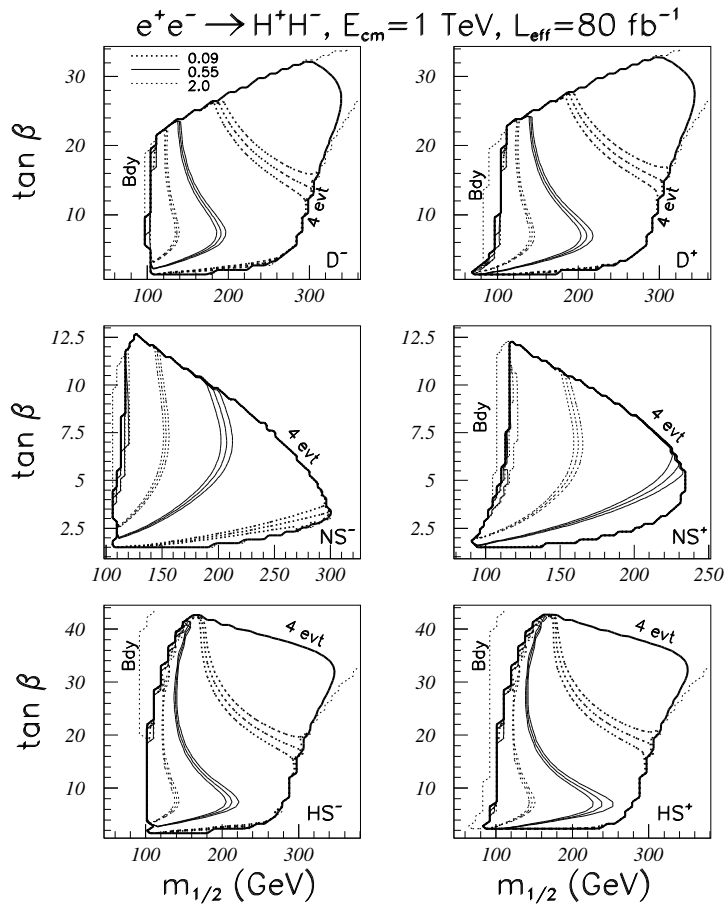


Figure 13: As in Fig. 9, but for the ratio of Eq. (6).

$$2*B(H^+ \rightarrow \tau^+\nu)/B(H^+ \rightarrow tb)$$

$$e^+e^- \rightarrow H^+H^-, E_{cm}=1 \text{ TeV}, L_{eff}=80 \text{ fb}^{-1}$$

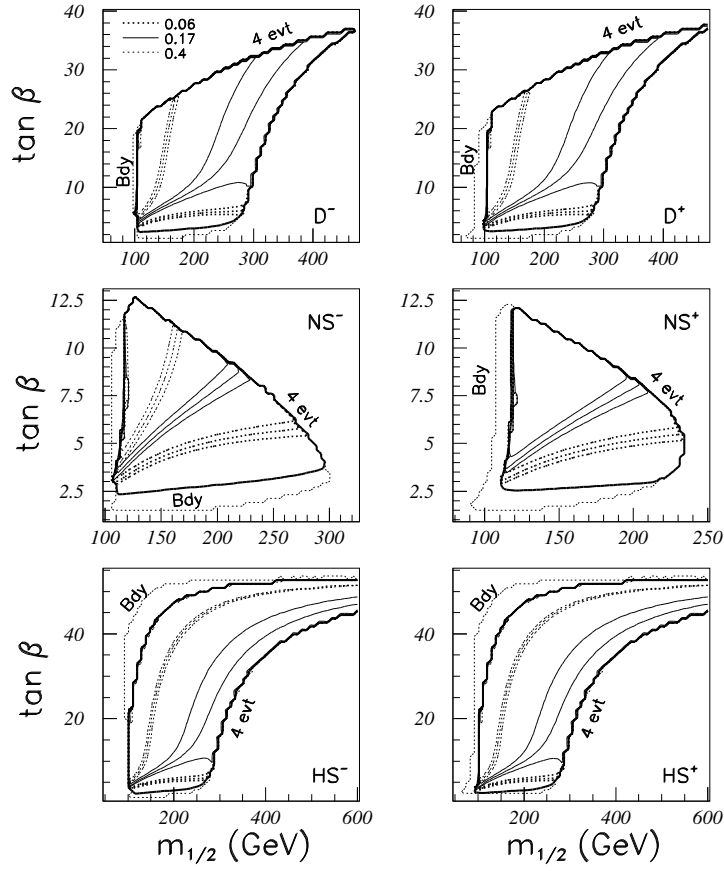


Figure 14: As in Fig. 9, but for the ratio of Eq. (7).

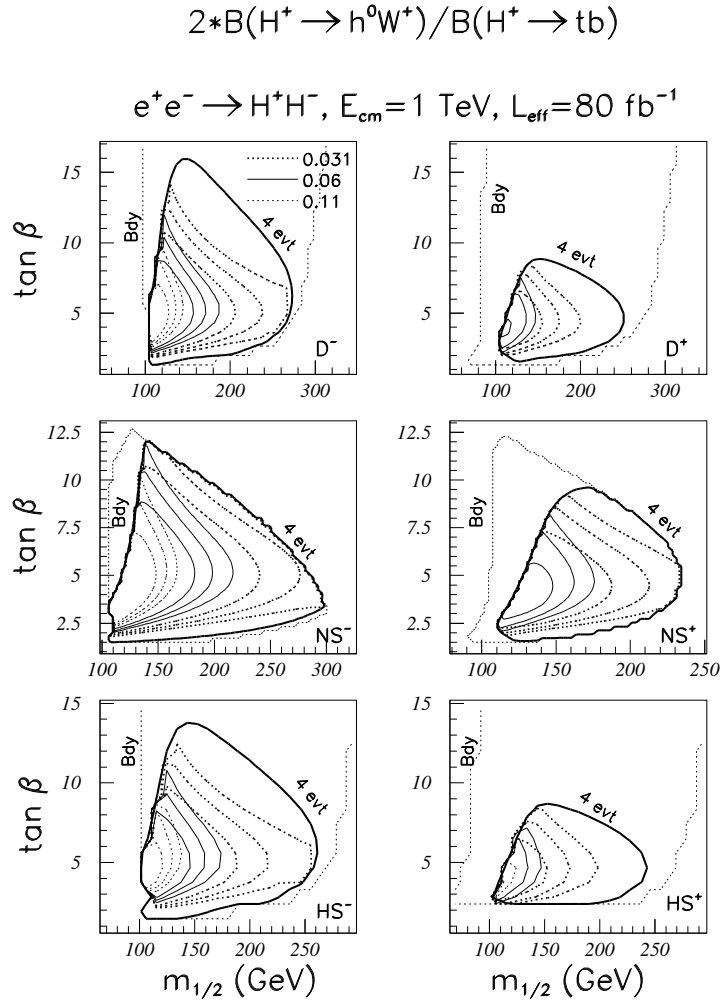


Figure 15: As in Fig. 9, but for the ratio of Eq. (8).

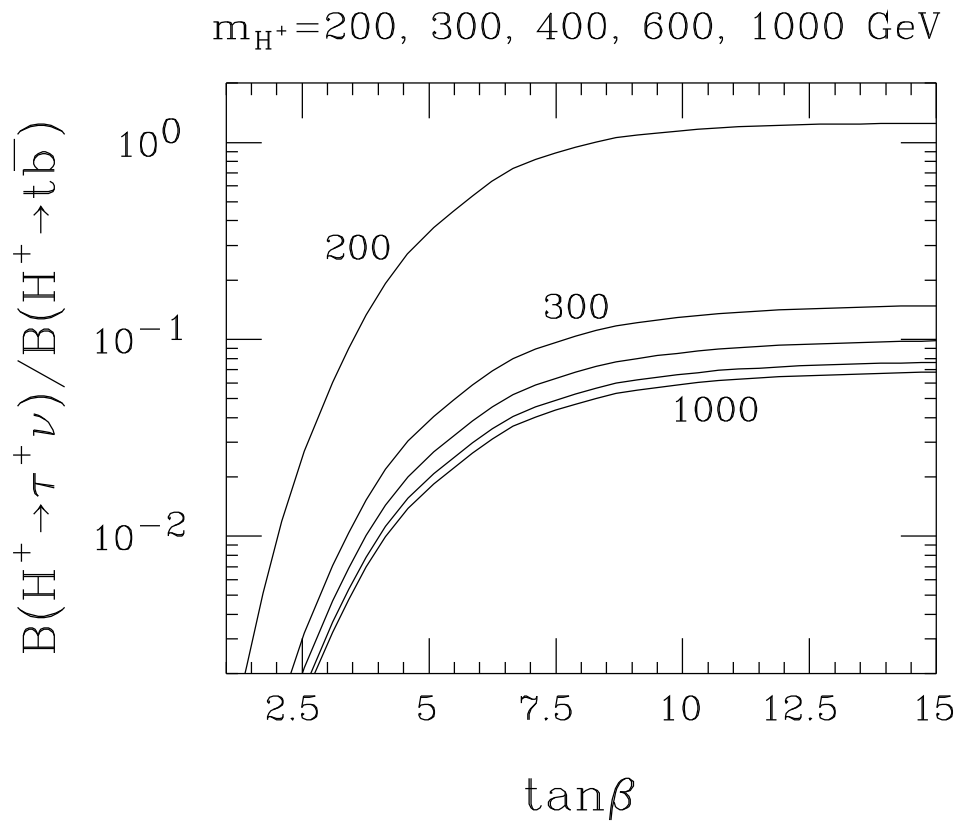


Figure 16: The ratio  $B(H^+ \rightarrow \tau^+ \nu) / B(H^+ \rightarrow t \bar{b})$  computed at tree level for  $m_t = 175 \text{ GeV}$  and  $m_b = 4 \text{ GeV}$  as a function of  $\tan\beta$  for  $m_{H^+} = 200, 300, 400, 600, \text{ and } 1000 \text{ GeV}$ .

$$2*B(H^+ \rightarrow \tau^+ \nu)/B(H^+ \rightarrow tb)$$

$$e^+e^- \rightarrow H^+H^-, E_{cm}=1 \text{ TeV}, L_{eff}=80 \text{ fb}^{-1}$$

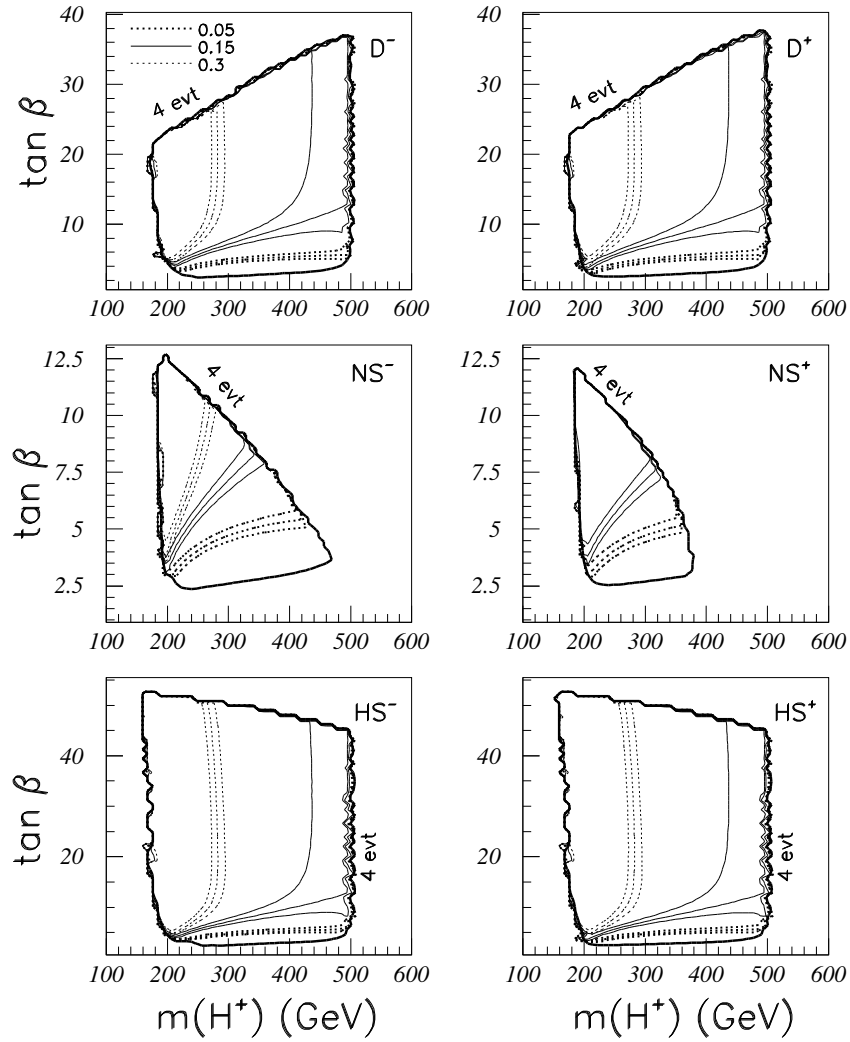


Figure 17: Contours of the ratio  $B(H^+ \rightarrow \tau^+ \nu)/B(H^+ \rightarrow tb)$  and its associated 1 contours are plotted as a function of  $\tan \beta$  and  $m_{H^+}$  for  $L_e = 80 \text{ fb}^{-1}$  at 1 TeV.

$$2 \langle B(H^0, A^0 \rightarrow t\bar{t}) / B(H^0, A^0 \rightarrow b\bar{b}) \rangle$$

$$e^+e^- \rightarrow H^0 A^0, E_{cm} = 1 \text{ TeV}, L_{eff} = 80 \text{ fb}^{-1}$$

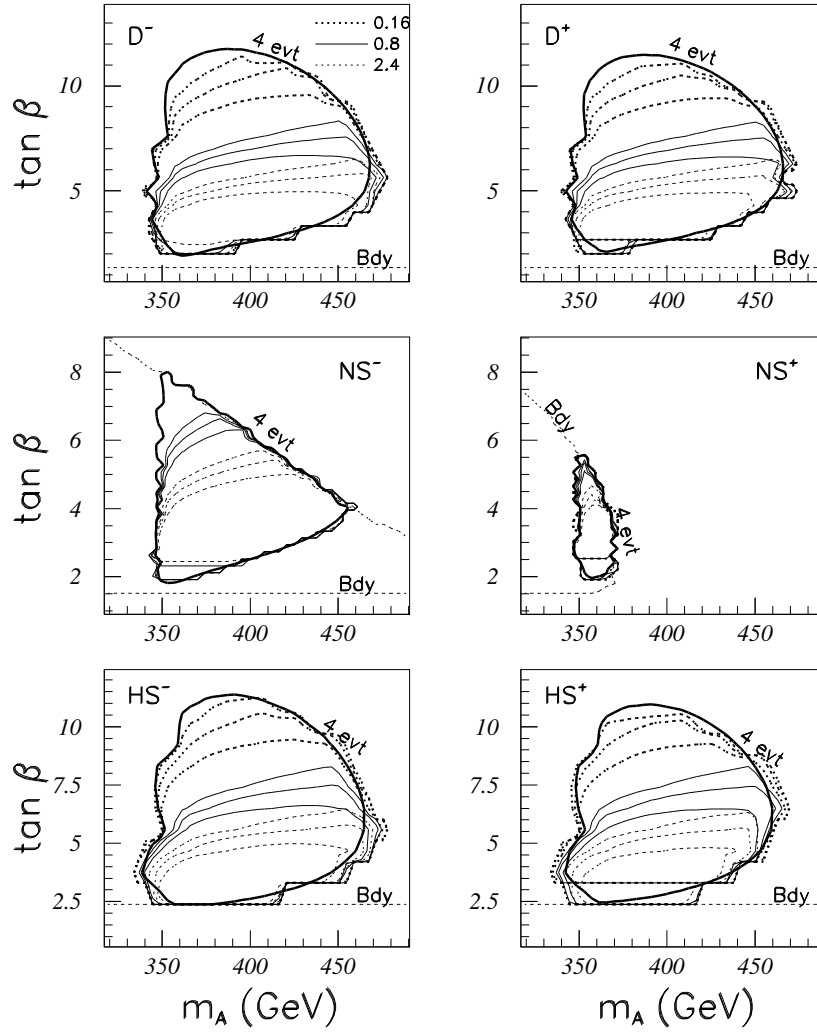


Figure 18: Contour of the ratio  $2\langle B(H^0, A^0 \rightarrow t\bar{t})/B(H^0, A^0 \rightarrow b\bar{b}) \rangle$  is associated 1 contours are plotted as a function of  $\tan \beta$  and  $m_A$  for  $L_e = 80 \text{ fb}^{-1}$  at 1 TeV.

a change from horizontal to vertical contours as one moves from low  $\tan \beta$  and large  $m_{1=2}$  (equivalent to large  $m_{H^+}$ ) to high  $\tan \beta$  and small  $m_{1=2}$  (implying small  $m_{H^+}$ ). The horizontal nature of the contours at large  $m_{1=2}; m_{H^+}$  and small  $\tan \beta$  can be understood from Fig. 16. As already briefly noted, this figure shows that when  $\tan \beta$  is small, small changes in  $\tan \beta$  yield large changes in the ratio, whereas there is little sensitivity to changes in  $m_{H^+}$  at fixed  $\tan \beta$  when  $m_{H^+}$  is large. In contrast, for small  $m_{H^+}$  Fig. 16 shows that small changes in  $m_{H^+}$  produce large changes in the ratio, whereas there is almost no sensitivity to  $\tan \beta$  when  $\tan \beta$  is large. As a result the contours in Figs. 14 and 17 are vertical at small  $m_{H^+}$  when  $\tan \beta$  is large. The wide separation between the central and  $\pm 1$  contours when  $m_{1=2}$  and  $\tan \beta$  are both large is a reflection of the constancy of this ratio (as displayed in Fig. 16) when both  $\tan \beta$  and  $m_{H^+}$  are large. Outside the region where  $\tan \beta$  and  $m_{H^+}$  are both large, the  $t \rightarrow b \tau$  contours are roughly orthogonal to those for the two SUSY ratios discussed earlier.

In general, it is apparent that the contours for the ratios of Eqs. (2), (6) and (7) in the  $(m_{1=2}; \tan \beta)$  plane are all oriented rather differently. This means that, in combination, these three relative Higgs branching fractions provide a fairly powerful check of the consistency of a given model, as well as a very definite determination of the value of  $\tan \beta$  that is required for a particular value of  $m_{1=2}$  in the model. We have already noted that  $m_{1=2}$  will be accurately determined in a given model by the neutralino and chargino masses, and that the measured  $m_{A^0}$  will generally provide a  $\tan \beta$  determination. This determination of  $\tan \beta$  from the masses and the value for  $\tan \beta$  required for consistency with the above three ratios of branching fractions are usually not consistent with one another for an incorrect model choice.

Additional discrimination power between the correct and an incorrect model choice is possible if we resolve the SUSY rates in Eqs. (2) and (6) into final states with a fixed number of leptons plus any number of jets (including 0) plus missing energy. Thus, instead of the single ratio of Eq. (2), where SUSY was defined to be the sum over all supersymmetric decay channels, it will prove useful to consider the three ratios obtained by dividing SUSY into the (i)  $[0^+][0j]$ , (ii)  $[1^+][0j]$  and (iii)  $[2^+][0j]$  channels, where the  $[0j]$  notation indicates that states with any number of jets (including 0) are summed over. Rates with  $[3^+][0j]$  are negligible. Similarly, instead of the ratio of Eq. (6) we will consider the two ratios obtained by separating SUSY into the channels (i) or (ii) defined above. Rates with  $[2^+][0j]$  are negligible. All SUSY final states will have large missing energy. The observable SUSY ratios so obtained are not very closely correlated, and thus are unlikely to be consistent with one another and with the  $t \rightarrow b \tau$  ratio for any but the correct model choice.

Still more discrimination power can be achieved via the other branching fraction ratios defined in Eqs. (3), (4), (5), and (8). For example, we see from Fig. 10 that the  $t \rightarrow b \tau$  ratio is quite sensitive to  $\tan \beta$ . This is even clearer by displaying the contours in  $(m_{A^0}; \tan \beta)$  space, Fig. 18. The  $H^0 \rightarrow h^0 h^0 = H^0 \rightarrow b \bar{b}$ ,  $A^0 \rightarrow Z h^0 = A^0 \rightarrow b \bar{b}$  and  $H^+ \rightarrow W^+ h^0 = H^+ \rightarrow t \bar{b}$  ratios plotted in Figs. 11, 12 and

15, respectively, are also sensitive to  $\tan \beta$ . However, even more interesting is their sensitivity to the sign of the  $\mu$  parameter. All three ratios are much smaller for  $\mu > 0$  than for  $\mu < 0$  [at a fixed  $(m_{1=2}; \tan \beta)$  location]. These differences derive almost entirely from a large decrease in the  $H^0 \rightarrow h^0 h^0$ ,  $A^0 \rightarrow Z h^0$  and  $H^\pm \rightarrow W^\pm h^0$  couplings, respectively, as the sign of  $\mu$  is changed from + to -. (In the case of the  $H^0 \rightarrow h^0 h^0$  coupling, this decrease is largely due to the change of sign of a radiative correction to the vertex associated with top, bottom, stop and sbottom loops. In the  $A^0 \rightarrow Z h^0$  and  $H^\pm \rightarrow W^\pm h^0$  cases, the large decrease is a tree-level effect.) Together, these three ratios will provide significant discrimination between scenarios with the opposite sign of  $\mu$ .

### 4.3 Quantitative Strategy for Estimating Model Discrimination Power

To determine the discrimination power achieved by all these ratios, we adopt an experimental point of view. We will choose a particular input boundary condition scenario and particular values of  $m_{1=2}$  and  $\tan \beta$  as 'nature's choice'. The resulting model will predict certain  $m_{A^0}$  and  $m_{e_1}$  values, which will be measured with small errors. The same values for these two observable masses can only be obtained for very specific  $m_{1=2}$  and  $\tan \beta$  values in any other boundary condition scenario. Once, the  $(m_{1=2}; \tan \beta)$  location in each scenario that yields the observed  $m_{A^0}$  and  $m_{e_1}$  is established, we compute the predictions for all the ratios of branching fractions. We use the notation  $R_i$ , with  $i$  specifying any particular ratio; the values of the  $R_i$  for the input scenario will be denoted by  $R_i^0$ . We also compute the 1- $\sigma$  error in the measurement of each of these ratios (denoted  $\Delta R_i$ ) as found assuming that the input model is nature's choice. We may then compute the expected  $\chi^2$  for any of the other models relative to the input model as:

$$\chi^2 = \sum_i \frac{(R_i - R_i^0)^2}{\Delta R_i^2}; \text{ with } \Delta R_i^2 = \frac{(R_i - R_i^0)^2}{R_i^2} : \quad (11)$$

We will see that very large  $\chi^2$  values are typically associated with an incorrect choice of model.

It is important to note that many other observables that discriminate between models will be available from other experimental observations. An additional  $\chi^2$  contribution should be added for each observable in assessing the overall improbability of a model other than the correct one. However, there are advantages to restricting oneself to the branching fraction ratios only. For example,  $m_{e_R}$  (which will be readily measured in slepton pair production) differs substantially at fixed  $m_{A^0}; m_{1=2}$  as one moves between the NS, D and HS scenarios, and would readily distinguish between the models. However,  $m_{e_R}$  is primarily sensitive to the value of the slepton  $m_0$  at  $M_U$ , which could differ from the  $m_0$  associated with the Higgs fields if the GUT boundary conditions are nonuniversal. In contrast, the branching fraction ratios are primarily sensitive to the Higgs  $m_0$  value relative to  $m_{1=2}$ .

Different sets of observables will have maximal sensitivity to different subsets of the GUT scale boundary conditions. The Higgs branching fraction ratios should be very valuable in sorting out the correct relation between  $m_{1=2}$  and the  $m_0$  for the Higgs fields, and in determining  $\tan\beta$ .

#### 4.4 A Test Case

As a specific example, suppose the correct model is D with  $m_{1=2} = 201.7 \text{ GeV}$  and  $\tan\beta = 7.50$ . This would imply  $m_{A^0} = 349.7 \text{ GeV}$ ,  $m_{e_1} = 149.5 \text{ GeV}$ . The  $m_{1=2}$  and  $\tan\beta$  values required in order to reproduce these same  $m_{A^0}$  and  $m_{e_1}$  values in the other scenarios are listed in Table 1. Also given in this table are the predicted values of  $m_{H^0}$  and  $m_{e_R}$  for each scenario. In order to get a first feeling for event numbers and for the errors that might be expected for the ratios of interest, we give in Table 2 the numbers of events,  $N$  and  $D$ , predicted in each scenario for use in determining the numerators and denominators of Eqs. (2)–(5) and Eqs. (6)–(8), assuming  $L_e = 80 \text{ fb}^{-1}$  at  $\sqrt{s} = 1 \text{ TeV}$ . These numbers include the SUSY branching fractions,  $B_e$  of Eq. (1), and so forth following the itemized list of factors given earlier.<sup>4</sup>

Table 1: We tabulate the values of  $m_{1=2}$  (in GeV) and  $\tan\beta$  required in each of our six scenarios in order that  $m_{A^0} = 349.7 \text{ GeV}$  and  $m_{e_1} = 149.5 \text{ GeV}$ . Also given are the corresponding values of  $m_{H^0}$  and  $m_{e_R}$ . Masses are in GeV.

	D	D <sup>+</sup>	NS	NS <sup>+</sup>	HS	HS <sup>+</sup>
$m_{1=2}$	201.7	174.4	210.6	168.2	203.9	180.0
$\tan\beta$	7.50	2.94	3.24	2.04	12.06	3.83
$m_{H^0}$	350.3	355.8	353.9	359.0	350.1	353.2
$m_{e_R}$	146.7	127.5	91.0	73.9	222.9	197.4

From Table 2, we observe that the  $D_{(2)-(5)}$  event rates for the  $\tan\beta > 0$  scenarios are all rather small as compared to the event rates for the  $\tan\beta < 0$  scenarios. (This happens because the  $m_{1=2}$  and  $\tan\beta$  values required for  $m_{A^0} = 349.7 \text{ GeV}$  and  $m_{e_1} = 149.5 \text{ GeV}$  when  $\tan\beta > 0$  are very close to the scenario boundary.) For example, if the D model is nature's choice, the  $H^0 A^0$ -pair denominator rates would be 198, implying a statistical error of only  $\sqrt{198} \approx 14$ . Assuming systematic error of order 10%, the net error in event number would certainly be  $< 35$ , i.e. many away from any of the  $\tan\beta > 0$  scenario predictions. We also see significantly larger

<sup>4</sup>Because  $B(A^0 \rightarrow t\bar{t}) = 0$  and  $B(H^0 \rightarrow t\bar{t})$  is typically small for the test case choice of  $m_{A^0} = 349.7 \text{ GeV}$  (given  $m_t = 175 \text{ GeV}$ ), the ratio of Eq. (3) and its numerator event rate are both small. Note that  $B_e(A^0 \rightarrow b\bar{b} + t\bar{t}) = B(A^0 \rightarrow b\bar{b})$  and that  $B_e(H^0 \rightarrow b\bar{b} + t\bar{t})$  is not very different from  $B(H^0 \rightarrow b\bar{b})$  for this same reason.

Table 2: We give the numbers of events predicted in each scenario at the parameter space locations specified in Table 1 available for determining the numerators and denominators of Eqs. (2)–(5) and Eqs. (6)–(8). These event rates are those for  $L_e = 80 \text{ fb}^{-1}$  at  $\sqrt{s} = 1 \text{ TeV}$ . They include all branching fractions. Our notation is  $N_{(\#)}$  and  $D_{(\#)}$  for the event rates in the numerator and denominator, respectively, of the ratio defined in Eq. ( $\#$ ).

	D	D <sup>+</sup>	NS	NS <sup>+</sup>	HS	HS <sup>+</sup>
$N_{(2)}$	97.0	92.3	88.3	49.2	76.1	124.0
$N_{(3)}$	0.1	0.7	3.8	1.02	0.0	0.2
$N_{(4)}$	16.4	2.7	46.6	1.47	3.8	2.4
$N_{(5)}$	2.0	1.3	9.2	0.6	0.4	1.1
$D_{(2)}$	198	9.6	62.1	2.6	250	18.2
$D_{(3)-(5)}$	198	8.9	58.3	1.6	250	18.0
$N_{(6)}$	225	189	138	135	189	262
$N_{(7)}$	58.4	4.2	6.5	1.1	90.0	9.5
$N_{(8)}$	13.0	12.8	21.9	9.0	3.3	12.3
$D_{(6)-(8)}$	317	415	445	465	320	348

numerator rates  $N_{(4)}$  and  $N_{(7)}$  for the  $< 0$  scenarios than for the  $> 0$  scenarios. Thus, in this particular case, even before examining the branching fraction ratios, the  $> 0$  scenarios could be excluded.

The  $N$  and  $D$  event numbers of Table 2 also make apparent the accuracy with which the ratios of Eqs. (2)–(5) and Eqs. (6)–(8) can be measured. For example, the event numbers  $N_2$  and  $D_2$  show that good statistical precision,  $\sim 10\%$ – $15\%$ , can be expected for the ratio of Eq. (2) in the  $< 0$  scenarios. Such statistical precision implies that this ratio will also clearly distinguish between the input  $D$  scenario and any of the  $> 0$  model predictions.

To illustrate the value of the branching fraction ratios more clearly, we present in Fig. 19 a plot which gives the expected values and the  $\pm 1$  errors as a function of scenario for four of the ratios that will be useful in distinguishing between the different scenarios at the given input (measured) values of  $m_{A^0}$  and  $m_{e_1}$ . In this plot, the errors as a function of scenario are those that are expected if the scenario listed on the horizontal axis is the correct one. Thus, if the correct model is  $D$ , the central value and  $\pm 1$  upper and lower limits for each ratio are those given above the  $D$  scenario label on the x-axis. The ability of each ratio to discriminate between a given scenario on the horizontal axis and one of the five alternatives is indicated by the extent to which the  $\pm 1$  error bars for the given scenario do not overlap the central points for the other scenario. Referring to Fig. 19 we observe the following.

## Scenario Overlap of Branching Fraction Ratios

$$E_{\text{cm}} = 1 \text{ TeV}, L_{\text{eff}} = 80 \text{ fb}^{-1}$$

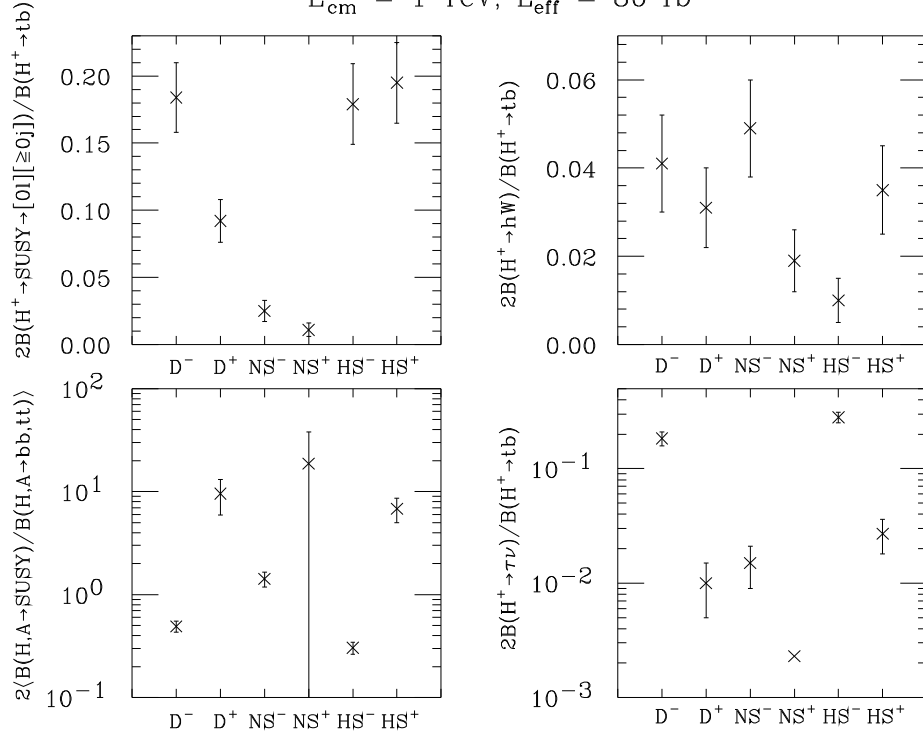


Figure 19: We plot the branching fraction ratios  $B(H^+ \rightarrow \text{SUSY} \rightarrow [0l][0j])/B(H^+ \rightarrow t\bar{b})$ ,  $B(H^+ \rightarrow \text{SUSY} \rightarrow [0l][0j])/B(H^+ \rightarrow t\bar{b})$ ,  $B(H^0; A^0 \rightarrow \text{SUSY})/B_e(H^0; A^0 \rightarrow b\bar{b}; t\bar{t})$  and  $B(H^+ \rightarrow h^0 W^+)/B(H^+ \rightarrow t\bar{b})$  with  $\pm 1$  error bars as a function of scenario, adjusting  $m_{1=2}$  and  $\tan\beta$  in each scenario so that  $m_{A^0} = 349.7 \text{ GeV}$  and  $m_{e_1} = 149.5 \text{ GeV}$  are held fixed. Error bars are for  $L_e = 80 \text{ fb}^{-1}$  at  $\sqrt{s} = 1 \text{ TeV}$ , and are those that would arise if the input (nature's choice) scenario is that listed on the horizontal axis. No error bar is shown for the  $H^+ \rightarrow t\bar{b}$  ratio in the  $NS^+$  scenario since the predicted rate is less than 4 events; a very large error bar should be assumed.

The ratio  $B(H^+ \rightarrow \text{SUSY} \rightarrow [0][0]) = B(H^+ \rightarrow \bar{t}b)$  succeeds in distinguishing the  $D^-$  scenario from all but the  $HS^-$  and  $HS^+$  scenarios.

The ratio  $B(H^+ \rightarrow \tau^+ \nu_\tau) = B(H^+ \rightarrow \bar{t}b)$  provides excellent discrimination between the  $D^-$  input scenario and the  $D^+$ ,  $NS^-$ ,  $NS^+$ , and  $HS^+$  scenarios, all of which must have  $\tan\beta < 4$  (in order to reproduce  $m_{A^0} = 349.7 \text{ GeV}$ ;  $m_{e_1} = 149.5 \text{ GeV}$ ) as compared to  $\tan\beta = 7.5$  for the  $D^-$  scenario. The much smaller  $\tan\beta$  values imply much smaller  $\tau^+ \nu_\tau = \bar{t}b$  ratios, as was illustrated in Fig. 16. The more limited ability of this ratio to discriminate between the high  $\tan\beta$  values of 7.5 for  $D^-$  vs. 12 for  $HS^-$  is also apparent from Fig. 16.

The ratio  $B(H^0; A^0 \rightarrow \text{SUSY}) = B(H^0; A^0 \rightarrow b\bar{b}; t\bar{t})$  will strongly rule out  $\tan\beta > 0$  scenarios if  $\tan\beta < 0$  is nature's choice. Due to the small error bars, this ratio provides some discrimination between the  $D^-$  and  $HS^-$  scenarios even though the predicted central values are not very different.

The ratio  $B(H^+ \rightarrow h^0 W^+) = B(H^+ \rightarrow \bar{t}b)$  is quite different for the  $D^-$ ,  $NS^-$ , and  $HS^+$  scenarios as compared to the  $D^+$ ,  $NS^+$ , and  $HS^-$  scenarios. However, discrimination power is limited by the relatively large error bars. Nonetheless, this ratio yields a bit more than 2:1 discrimination against the  $HS^-$  model if the  $D^-$  model is nature's choice.

The quite substantial dependence of the ratios on scenario and location in parameter space, as displayed in Figs. 9, 10, 11, 12, 13, 14, and 15, suggests that similar discrimination will be possible from most input scenario and parameter space location choices.

In Table 3 we more thoroughly quantify the process of excluding the  $D^+$ ,  $NS^-$ ,  $NS^+$ ,  $HS^-$ , and  $HS^+$  scenarios relative to the input  $D^-$  scenario. There we give the contribution to  $\chi^2$  (computed relative to the assumed-to-be-correct  $D^-$  scenario) for each of a selection of independently measurable ratios. Also given for each of the incorrect scenarios is the sum of these contributions. This table shows that the  $D^-$  scenario can be distinguished from the  $D^+$ ,  $NS^-$ ,  $NS^+$ , and  $HS^+$  scenarios at an extremely high statistical level. Further, even though no one of the branching fraction ratios provides an absolutely clear discrimination between the  $D^-$  and the  $HS^-$  scenarios, the accumulated discrimination power obtained by considering all the ratios is very substantial. In particular, although the ratios of Eq. (4), (5), and (8) are only poorly measured for  $L_e = 80 \text{ fb}^{-1}$ , their accumulated  $\chi^2$  weight can be an important component in determining the likelihood of a given model and thereby ruling out incorrect model choices.

Thus, consistency of all the ratios with one another and with the measured  $m_{A^0}$ , neutralino and chargino masses will generally restrict the allowed models to ones that are very closely related. The likelihood or probability associated with the best fit to all these observables in a model that differs significantly from the correct model would be very small.

Table 3: We tabulate  $\frac{R_i^2}{i}$ , see Eq. (11), (relative to the D scenario) for the indicated branching fraction ratios as a function of scenario, assuming the measured  $m_{A^0}$  and  $m_{\tilde{e}_1}$  values are 349.7 GeV and 149.5 GeV, respectively. The SUSY channels have been resolved into final states involving a fixed number of leptons. The error used in calculating each  $\frac{R_i^2}{i}$  is the approximate 1  $\sigma$  error (as defined in text) with which the given ratio  $R_i$  could be measured for  $L_e = 80 \text{ fb}^{-1}$  at  $\sqrt{s} = 1 \text{ TeV}$  assuming that the D scenario is the correct one.

Ratio	D	D <sup>+</sup>	NS	NS <sup>+</sup>	HS	HS <sup>+</sup>
$2\text{hB}(H^0; A^0 \rightarrow \text{SUSY} \rightarrow [0][0j]) = \frac{B_e(H^0; A^0 \rightarrow b\bar{b}; \tilde{t}\tilde{t})}{B_e(H^0; A^0 \rightarrow b\bar{b}; \tilde{t}\tilde{t})}$	0	12878	1277	25243	0.77	10331
$2\text{hB}(H^0; A^0 \rightarrow \text{SUSY} \rightarrow [1][0j]) = \frac{B_e(H^0; A^0 \rightarrow b\bar{b}; \tilde{t}\tilde{t})}{B_e(H^0; A^0 \rightarrow b\bar{b}; \tilde{t}\tilde{t})}$	0	13081	2.41	5130	3.6	4783
$2\text{hB}(H^0; A^0 \rightarrow \text{SUSY} \rightarrow [2][0j]) = \frac{B_e(H^0; A^0 \rightarrow b\bar{b}; \tilde{t}\tilde{t})}{B_e(H^0; A^0 \rightarrow b\bar{b}; \tilde{t}\tilde{t})}$	0	4543	5.12	92395	26.6	116
$B(H^0 \rightarrow h^0 h^0) = B(H^0 \rightarrow b\bar{b})$	0	109	1130	1516	10.2	6.2
$2B(H^+ \rightarrow \text{SUSY} \rightarrow [0][0j]) = \frac{B(H^+ \rightarrow \tilde{t}\tilde{b})}{B(H^+ \rightarrow \tilde{t}\tilde{b})}$	0	12.2	36.5	43.2	0.04	0.2
$2B(H^+ \rightarrow \text{SUSY} \rightarrow [1][0j]) = \frac{B(H^+ \rightarrow \tilde{t}\tilde{b})}{B(H^+ \rightarrow \tilde{t}\tilde{b})}$	0	1.5	0.3	0.1	5.6	0.06
$2B(H^+ \rightarrow h^0 W) = B(H^+ \rightarrow \tilde{t}\tilde{b})$	0	0.8	0.5	3.6	7.3	0.3
$2B(H^+ \rightarrow \tilde{\nu}_e) = B(H^+ \rightarrow \tilde{t}\tilde{b})$	0	43.7	41.5	47.7	13.7	35.5
$\frac{R_i^2}{i}$	0	30669	2493	124379	68	15272

## 4.5 Separating Different SUSY Decay Modes

An important issue is the extent to which one can be sensitive to the branching fractions for different types of SUSY decays of the Higgs bosons, relative to one another and relative to the overall SUSY decay branching fraction. Interesting SUSY decay rates include:

$B(H^0; A^0 \rightarrow \tilde{e}_1^0 \tilde{e}_1^0 + e e)$ , leading to a totally invisible final state;

$B(H^0; A^0 \rightarrow \tilde{\chi}^+ \tilde{\chi}^-)$ , where  $\tilde{\chi} \rightarrow \tilde{\nu}_e$  or  $\tilde{e}_1$ ;

$B(H^0; A^0 \rightarrow \tilde{e}_1^+ \tilde{e}_1^-)$ , where  $\tilde{e}_1 \rightarrow \tilde{\nu}_e$ ,  $j \tilde{e}_1^0$  or  $\tilde{\chi} e$  (with  $\tilde{\chi} e \rightarrow \tilde{\nu}_e \tilde{e}_1^0$ );

$B(H \rightarrow \tilde{\chi} e)$ , where  $\tilde{\chi} \rightarrow \tilde{\nu}_e$ , or  $\tilde{e}_1$ ;

$B(H \rightarrow \tilde{e}_1 \tilde{e}_1^0)$ , where  $\tilde{e}_1 \rightarrow \tilde{\nu}_e$ ,  $j \tilde{e}_1^0$  or  $\tilde{\chi} e$  (with  $\tilde{\chi} e \rightarrow \tilde{\nu}_e \tilde{e}_1^0$ ).

Predictions for such rates depend in a rather detailed fashion upon the SUSY parameters and would provide valuable information regarding the SUSY scenario. For example, in going from NS to D to HS the masses of the sneutrinos and sleptons increase relative to those for the charginos and neutralinos. The  $H^0; A^0 \rightarrow \tilde{\chi}^+ \tilde{\chi}^-$  and  $H \rightarrow \tilde{\chi} e$  branching fractions should decline in comparison to  $H^0; A^0 \rightarrow$

$e_1^+ e_1$  and  $H^0 \rightarrow e_1 e_1^0$ , respectively. In small sections of the D and NS scenario parameter spaces, the sleptons and sneutrinos are sufficiently light that  $e_1$  decays almost exclusively to  $\tilde{e} e$  followed by  $\tilde{e} e \rightarrow \tilde{\nu} e_1^0 e_1^0$ , implying that  $e_1$  decays would mainly yield leptons and not jets.

The difficulty is that several different SUSY channels can contribute to any given final state. Two examples were noted earlier: the  $\tilde{\nu} \tilde{\nu} + E_T$  channel receives contributions from both  $H^0; A^0 \rightarrow \tilde{e}^+ \tilde{e}$  and  $e_1^+ e_1$  decays; and the  $\tilde{\nu} + E_T$  channel receives contributions from  $H^0 \rightarrow \tilde{e} e$  and  $e_1 e_1^0$ . Another example, is the purely invisible  $H^0$  or  $A^0$  final state; it can arise from either  $e_1^0 e_1^0$  or  $ee$  (with  $e \rightarrow e_1^0$ ) production. Thus, the physically distinct channels, defined by the number of leptons and jets present,<sup>5</sup> typically have multiple sources. Still, a comparison between the rates for the final states so-defined might be quite revealing. For instance, if  $e_1 \rightarrow \tilde{e} e$  is not kinematically allowed, the  $e_1^+ e_1$  final states are expected to yield more  $1\tilde{\nu} + 2j$  and  $0\tilde{\nu} + 4j$  events than  $2\tilde{\nu} + 0j$  events, whereas  $\tilde{e}^+ \tilde{e}$  events will yield only  $2\tilde{\nu} + 0j$  events. Further, the  $\tilde{\nu}$ s must be of the same type in this latter case. The effective branching fraction for  $e_1^+ e_1 \rightarrow \tilde{\nu} \tilde{\nu} + E_T$  with both  $\tilde{\nu}$ s of the same type is only 1/81. In addition, the  $\tilde{\nu}$ s in the latter derive from three-body decays of the  $e_1$ , and would be much softer on average than  $\tilde{\nu}$ s from  $\tilde{e}^+ \tilde{e}$ . Even if this difference is difficult to see directly via distributions, it will lead to higher efficiency for picking up the  $\tilde{e}^+ \tilde{e}$  events. Of course, if event numbers are sufficiently large (which in general they are not) that detailed kinematical distributions within each final state could be obtained, they would provide additional information. We do not pursue this latter possibility here.

Based on the above discussion, the following ratios would appear to be potentially useful. For the  $H^0$  and  $A^0$  we consider:

$$\frac{B(H^0 \rightarrow b\bar{b})B(A^0 \rightarrow [0\tilde{\nu}][0j]) + B(A^0 \rightarrow b\bar{b})B(H^0 \rightarrow [0\tilde{\nu}][0j])}{B(H^0 \rightarrow b\bar{b})B(A^0 \rightarrow \text{SUSY}) + B(A^0 \rightarrow b\bar{b})B(H^0 \rightarrow \text{SUSY})}; \quad (12)$$

$$\frac{B(H^0 \rightarrow b\bar{b})B(A^0 \rightarrow [2\tilde{\nu}][0j]) + B(A^0 \rightarrow b\bar{b})B(H^0 \rightarrow [2\tilde{\nu}][0j])}{B(H^0 \rightarrow b\bar{b})B(A^0 \rightarrow \text{SUSY}) + B(A^0 \rightarrow b\bar{b})B(H^0 \rightarrow \text{SUSY})}; \quad (13)$$

$$\frac{B(H^0 \rightarrow b\bar{b})B(A^0 \rightarrow [10\tilde{\nu}][0j]) + B(A^0 \rightarrow b\bar{b})B(H^0 \rightarrow [10\tilde{\nu}][0j])}{B(H^0 \rightarrow b\bar{b})B(A^0 \rightarrow \text{SUSY}) + B(A^0 \rightarrow b\bar{b})B(H^0 \rightarrow \text{SUSY})}; \quad (14)$$

$$\frac{B(H^0 \rightarrow b\bar{b})B(A^0 \rightarrow [0\tilde{\nu}][1j]) + B(A^0 \rightarrow b\bar{b})B(H^0 \rightarrow [0\tilde{\nu}][1j])}{B(H^0 \rightarrow b\bar{b})B(A^0 \rightarrow \text{SUSY}) + B(A^0 \rightarrow b\bar{b})B(H^0 \rightarrow \text{SUSY})}; \quad (15)$$

$$\frac{B(H^0 \rightarrow b\bar{b})B(A^0 \rightarrow [1\tilde{\nu}][1j]) + B(A^0 \rightarrow b\bar{b})B(H^0 \rightarrow [1\tilde{\nu}][1j])}{B(H^0 \rightarrow b\bar{b})B(A^0 \rightarrow \text{SUSY}) + B(A^0 \rightarrow b\bar{b})B(H^0 \rightarrow \text{SUSY})}; \quad (16)$$

(As before,  $m_{A^0} = m_{H^0}$  implies that we cannot separate the  $H^0$  and  $A^0$  via the tagging procedure.<sup>6</sup>) Once again, we employ shorthand notations for the quantities

<sup>5</sup>The totally invisible final state would be  $[0\tilde{\nu}][0j]$ , and so forth.

<sup>6</sup>The  $A^0 \rightarrow \tilde{e}^+ \tilde{e}$  branching ratio turns out to be rather small in the three GUT scenarios studied | the required L-R mixing is numerically very small in the slepton sector.

appearing in Eqs. (12)–(16). For example, the ratio of Eq. (12) will be denoted by

$$\frac{hB(A^0; H^0 \rightarrow [\ell^+][\ell^-])B(H^0; A^0 \rightarrow b\bar{b})}{hB(A^0; H^0 \rightarrow \text{SUSY})B(H^0; A^0 \rightarrow b\bar{b})} \quad \text{or} \quad \frac{B(H^0; A^0 \rightarrow [\ell^+][\ell^-])}{B(H^0; A^0 \rightarrow \text{SUSY})} \quad (17)$$

in what follows.

For the  $H^\pm$  we consider the ratios:

$$\frac{B(H^+ \rightarrow [\ell^+][\ell^-])B(H^\pm \rightarrow b\bar{t}) + B(H^\pm \rightarrow [\ell^+][\ell^-])B(H^+ \rightarrow t\bar{b})}{B(H^+ \rightarrow \text{SUSY})B(H^\pm \rightarrow b\bar{t}) + B(H^\pm \rightarrow \text{SUSY})B(H^+ \rightarrow t\bar{b})}; \quad (18)$$

$$\frac{B(H^+ \rightarrow [\ell^+][\ell^-])B(H^\pm \rightarrow b\bar{t}) + B(H^\pm \rightarrow [\ell^+][\ell^-])B(H^+ \rightarrow t\bar{b})}{B(H^+ \rightarrow \text{SUSY})B(H^\pm \rightarrow b\bar{t}) + B(H^\pm \rightarrow \text{SUSY})B(H^+ \rightarrow t\bar{b})}; \quad (19)$$

$$\frac{B(H^+ \rightarrow [\ell^+][\ell^-])B(H^\pm \rightarrow b\bar{t}) + B(H^\pm \rightarrow [\ell^+][\ell^-])B(H^+ \rightarrow t\bar{b})}{B(H^+ \rightarrow \text{SUSY})B(H^\pm \rightarrow b\bar{t}) + B(H^\pm \rightarrow \text{SUSY})B(H^+ \rightarrow t\bar{b})}; \quad (20)$$

The ratios of Eqs. (18)–(20) reduce to:

$$\frac{B(H^+ \rightarrow [\ell^+][\ell^-])}{B(H^+ \rightarrow \text{SUSY})}; \quad \frac{B(H^+ \rightarrow [\ell^+][\ell^-])}{B(H^+ \rightarrow \text{SUSY})}; \quad \frac{B(H^+ \rightarrow [\ell^+][\ell^-])}{B(H^+ \rightarrow \text{SUSY})}; \quad (21)$$

respectively.

Also of interest are ratios of the different numerator terms to one another within the above neutral and charged Higgs boson sets. All the ratios that one can form have the potential to provide important tests of the Higgs decays to the supersymmetric particle pair final states.

To illustrate, we present two figures. In Fig. 20 we present three-dimensional lego plots of the ratio of Eq. (14) as a function of location in  $(m_{1=2}; \tan\beta)$  parameter space. (Because of the combination of slow variation and very sharp changes, the contour plots similar to those presented earlier are rather difficult to interpret.) In Fig. 21, we plot the numerator of Eq. (19) divided by the numerator of Eq. (20). In both sets of lego plots, the ratio is set to zero if there are fewer than 4 events in the numerator or denominator after including the earlier-discussed tagging/reconstruction efficiencies and assuming  $\sqrt{s} = 1 \text{ TeV}$  and  $L_e = 80 \text{ fb}^{-1}$ .

The most important feature apparent from these figures is the generally decreasing magnitude of these two ratios as one moves from the NS to the D to the HS scenario. This is a result of the decreasing importance of slepton/sneutrino-related decays as compared to chargino/neutralino-based decays. When the latter types of decay are prevalent, a much larger fraction of the events will have jets than if the former decays dominate. The decreasing importance of the slepton/sneutrino class is to be expected due to the increasing mass of these states as  $m_0$  increases in going from NS to D to HS. The occasionally very large values of  $B(H^+ \rightarrow [\ell^+][\ell^-]) = B(H^+ \rightarrow [\ell^+][\ell^-])$  in Fig. 21 in the D and NS<sup>+</sup> plots occur in the small wedges of parameter space where  $e_1 \rightarrow e^+e^-$  decays are kinematically

$$\frac{\langle B(H^0, A^0 \rightarrow \text{SUSY} \rightarrow [nl][0j])B(A^0, H^0 \rightarrow bb) \rangle}{\langle B(H^0, A^0 \rightarrow \text{SUSY})B(A^0, H^0 \rightarrow bb) \rangle}$$

$$e^+e^- \rightarrow H^0 A^0, E_{cm}=1 \text{ TeV}, L_{eff}=80 \text{ fb}^{-1}$$

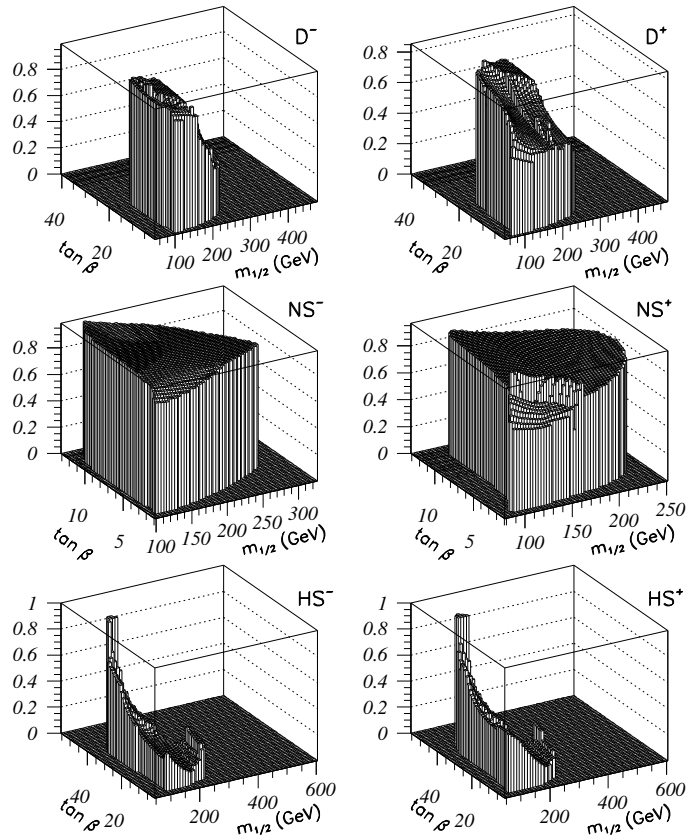


Figure 20: We present lego plots of the ratio of Eq. (14) in each of the six scenarios as a function of location in  $(m_{1/2}; \tan \beta)$  parameter space. The value of the ratio is given by the height on the z-axis. Non-zero values of the ratio are given only in regions where there are at least 4 events in the numerator after including tagging/reconstruction efficiencies.

$$B(H^+ \rightarrow \text{SUSY} \rightarrow [\geq 1j][0j]) / B(H^+ \rightarrow \text{SUSY} \rightarrow [0j][\geq 1j])$$

$$e^+e^- \rightarrow H^+H^-, E_{\text{cm}}=1 \text{ TeV}, L_{\text{eff}}=80 \text{ fb}^{-1}$$

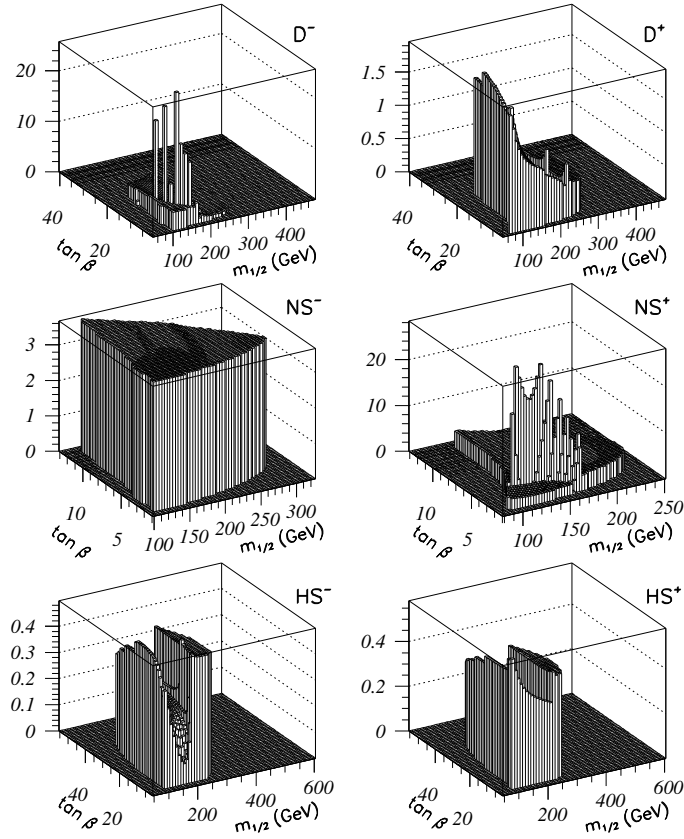


Figure 21: We present lego plots of the numerator of Eq. (19) divided by the numerator of Eq. (20) in each of the six scenarios as a function of location in  $(m_{1/2}; \tan \beta)$  parameter space. The value of the ratio is given by the height on the z-axis. Non-zero values of the ratio are given only in regions where there are at least 4 events in both the numerator and denominator after including tagging/reconstruction efficiencies.

allowed, and final states containing only jets must arise from higherino states and, thus, are very rare.

It should be apparent from these two figures that rather dramatic differences between the scenarios at a given  $(m_{1=2}; \tan \beta)$  location are the norm. In general, statistics are such that the different scenarios can be distinguished from one another at a substantial level of significance just on the basis of these two ratios. Ratios other than the two plotted ones can also provide good discrimination. We shall illustrate this for our standard  $m_{A^0} = 349.7 \text{ GeV}$ ;  $m_{e_1} = 149.5 \text{ GeV}$  point discussed in association with Tables 1 and 2, Fig. 19 and Table 3.

Table 1 gives the  $(m_{1=2}; \tan \beta)$  parameters required for  $m_{A^0} = 349.7 \text{ GeV}$ ;  $m_{e_1} = 149.5 \text{ GeV}$  in each of the six GUT scenarios. In Table 4 the event rates for the SUSY final states corresponding to the numerators of the ratios listed in Eqs. (12)–(16) and (18)–(20) are given for these  $(m_{1=2}; \tan \beta)$  values. We will follow the same notation in terms of  $N_{(\text{Eq.} \#)}$  as for Table 2. An examination of Table 4 reveals event rates in the individual channels that vary from a few events, implying poor statistics, to 50 or 60 events, for which statistical accuracy would be quite reasonable.

Table 4: For the  $(m_{1=2}; \tan \beta)$  values required for  $m_{A^0} = 349.7 \text{ GeV}$ ;  $m_{e_1} = 149.5 \text{ GeV}$ , we tabulate the numbers of events predicted in each scenario in the final states corresponding to the numerators and denominators of Eqs. (12)–(16) and (18)–(20). These rates are those obtained for  $L_e = 80 \text{ fb}^{-1}$  at  $\sqrt{s} = 1 \text{ TeV}$ . They include all branching fractions.

	D	D <sup>+</sup>	NS	NS <sup>+</sup>	HS	HS <sup>+</sup>
N <sub>(12)</sub>	14.8	20.4	64.3	8.7	7.7	14.7
N <sub>(13)</sub>	29.5	20.4	15.6	19.5	1.4	6.8
N <sub>(14)</sub>	53.7	43.3	79.8	30.2	9.1	21.7
N <sub>(15)</sub>	10.8	9.8	3.1	3.0	30.5	37.2
N <sub>(16)</sub>	10.8	19.3	1.8	3.4	5.6	22.1
D <sub>(12)–(16)</sub>	97.2	87.9	86.4	37.7	76.1	124
N <sub>(18)</sub>	26.0	24.3	40.6	40.5	13.4	25.9
N <sub>(19)</sub>	26.0	26.2	40.6	43.5	13.4	25.9
N <sub>(20)</sub>	58.4	38.3	11.1	5.2	57.2	67.9
D <sub>(18)–(20)</sub>	225	189	138	135	189	262

Not surprisingly, the ratios of rates of the various SUSY channels can contribute significantly to our ability to discriminate between different GUT scenarios. To illustrate, we follow the same procedure as in Table 3. Taking  $m_{A^0} = 349.7 \text{ GeV}$  and  $m_{e_1} = 149.5 \text{ GeV}$ , we assume that the correct scenario is D and compute the  $\chi^2$  by which the prediction for a given ratio in the other scenarios deviates

from the  $D^-$  prediction. Statistics are computed on the basis of the expected  $D^-$  rates, as given in Table 4. The resulting  $\chi^2$  values are given in Table 5. Since these ratios are not all statistically independent of one another, we do not sum their  $\chi^2$ 's to obtain an overall discrimination level. However, a rough indication of the level at which any given scenario can be ruled out relative to the  $D^-$  is obtained if we add the largest  $\chi^2$  from the neutral Higgs list and the largest from the charged Higgs list. The weakest discrimination level following this procedure is  $\chi^2 = 15$  in the case of the  $D^+$  scenario. Note that this scenario is highly unlikely on the basis of the earlier  $\chi^2$  value listed in Table 3. In Table 3, the weakest discrimination was that for the HS scenario with  $\chi^2 = 68$ . We observe from Table 5 that the ratio  $B(H^0; A^0 \rightarrow \tau^+ \tau^-) = B(H^0; A^0 \rightarrow \tau^+ \tau^-)$  has  $\chi^2 = 928$  for the HS case, which would certainly rule it out.

Table 5: We tabulate  $\chi^2$ , see Eq. (11), (relative to the  $D^-$  scenario) for the indicated ratios as a function of scenario, assuming the measured  $m_{A^0}$  and  $m_{\tilde{e}_1}$  values are 349.7 GeV and 149.5 GeV, respectively. The SUSY channels have been resolved into final states involving a restricted number of leptons and jets. Only those ratios with substantial power for discriminating between scenarios are tabulated. The error used in calculating each  $\chi^2$  is the approximate 1 $\sigma$  error (as defined in text) with which the given ratio  $R_i$  could be measured for  $L_e = 80 \text{ fb}^{-1}$  at  $\sqrt{s} = 1 \text{ TeV}$  assuming that the  $D^-$  scenario is the correct one.

Ratio	D	D <sup>+</sup>	NS	NS <sup>+</sup>	HS	HS <sup>+</sup>
$B(H^0; A^0 \rightarrow \tau^+ \tau^-) = B(H^0; A^0 \rightarrow \text{SUSY})$	0	3.5	193	3.4	1.4	0.6
$B(H^0; A^0 \rightarrow \tau^+ \tau^-) = B(H^0; A^0 \rightarrow \text{SUSY})$	0	0.4	15.3	6.8	20.9	15.8
$B(H^0; A^0 \rightarrow \tau^+ \tau^-) = B(H^0; A^0 \rightarrow \tau^+ \tau^-)$	0	9.6	503	0.1	928	105
$B(H^0; A^0 \rightarrow \tau^+ \tau^-) = B(H^0; A^0 \rightarrow \tau^+ \tau^-)$	0	5.8	41.9	0.03	48.4	24.5
$B(H^0; A^0 \rightarrow \tau^+ \tau^-) = B(H^0; A^0 \rightarrow \tau^+ \tau^-)$	0	1.4	1074	6.4	3.5	2.7
$B(H^0; A^0 \rightarrow \tau^+ \tau^-) = B(H^0; A^0 \rightarrow \tau^+ \tau^-)$	0	0.3	3520	4.3	0	1.4
$B(H^+ \rightarrow \tau^+ \tau^-) = B(H^+ \rightarrow \text{SUSY})$	0	1.0	56.2	75.2	3.4	0.5
$B(H^+ \rightarrow \tau^+ \tau^-) = B(H^+ \rightarrow \text{SUSY})$	0	2.1	21.7	33.4	1.3	0
$B(H^+ \rightarrow \tau^+ \tau^-) = B(H^+ \rightarrow \tau^+ \tau^-)$	0	5.2	930	5738	4.0	0.4

The above illustrations demonstrate that the ratios of rates for individual SUSY channels correlate strongly with the underlying physics of the different GUT scenarios (light vs. heavy sleptons in particular) and add a powerful component to our ability to determine the correct scenario.

## 5 Summary and Conclusions

In this paper, we have considered detecting and studying the heavy Higgs bosons of the minimal supersymmetric model when pair produced in  $e^+e^-$  or  $\tau^+\tau^-$

collisions. We have shown that, in the SUSY GUT models studied, the target luminosities of  $L = 200 \text{ fb}^{-1}$  and  $L = 1000 \text{ fb}^{-1}$  at  $\sqrt{s} = 1 \text{ TeV}$  and  $4 \text{ TeV}$ , respectively, will allow detection of  $H^0 A^0$  and  $H^+ H^-$  pair production throughout essentially all of the model parameter space which is allowed by theoretical and kinematic constraints, despite the presence of SUSY decay modes of the  $H^0; A^0; H^\pm$  at a significant level. The all-jet and high-multiplicity final states coming from  $H^0; A^0 \rightarrow b\bar{b}; t\bar{t}$  and  $H^\pm \rightarrow t\bar{b}; H^\pm \rightarrow b\bar{t}$  are essentially background free and provide appropriate and efficient signals with rates that are adequate even when SUSY decays are present. In the all-jet channels, the individual Higgs boson masses,  $m_{A^0}, m_{H^0}$  and  $m_{H^\pm}$ , can be measured and the approximate degeneracy ( $m_{A^0} \approx m_{H^0} \approx m_{H^\pm}$ ) predicted by the MSSM can be checked.

Once the Higgs bosons are detected and their masses determined, the relative branching fractions for the decay of a single Higgs boson can be measured by ‘tagging’ (i.e. identifying) one member of the  $H^0 A^0$  or  $H^+ H^-$  pair in an all-jet mode, and then looking at the ratios of the numbers of events in different event classes on the opposing side. In this way, the relative branching ratios of Eqs. (2)–(5), Eqs. (6)–(8), Eqs. (12)–(16), and Eqs. (18)–(15) can be measured with reasonable accuracy whenever parameters are such that the final states in the numerator and denominator both have significant event rate<sup>7</sup>. We find that the measured Higgs masses and relative branching fractions, in combination with direct measurements of the chargino and neutralino masses, will over-constrain and very strongly limit the possible SUSY GUT models.

The specific SUSY GUT models considered are moderately conservative in that they are characterized by universal boundary conditions. In all, we delineated expectations for six different models, requiring correct electroweak symmetry breaking via evolution from the GUT scale to  $m_Z$ . For each model, there are only two parameters:  $m_{1=2}$  (the universal gaugino) mass; and  $\tan\beta$  (the usual Higgs field vacuum expectation value ratio). Each model is characterized by a definite relation of the universal soft-SUSY-breaking scalar mass,  $m_0$ , and the universal mixing parameter,  $A_0$ , to  $m_{1=2}$ , as well as by a choice for the sign of  $\mu$  (the Higgs superfield mixing coefficient).

The strategy for checking the consistency of a given GUT hypothesis is straightforward. First, the measured  $A^0$ , neutralino and chargino masses are, in almost all cases, already sufficient to determine the  $m_{1=2}$  and  $\tan\beta$  values required in the given GUT scenario with good precision. The value of  $\tan\beta$  so obtained should agree with that determined from chargino pair production rates. The Higgs sector branching fractions can then be predicted and become an important testing ground for the consistency of the proposed GUT hypothesis as well as for testing the MSSM two-doublet Higgs sector structure *per se*.

<sup>7</sup>We focus on event rate ratios rather than the absolute rates in the many different channels since the possibly large systematic errors of the absolute rates will tend to cancel in the ratios. In some cases, absolute event rates are so different that they would also provide substantial discrimination between different models, despite the possibly large systematic errors.

Within the list of ratios of branching fractions given in Eqs. (2)–(5) and (6)–(8), the average<sup>8</sup>  $H^0; A^0 \rightarrow \text{SUSY}$ , the  $H^\pm \rightarrow \text{SUSY}$  and the  $H^\pm \rightarrow \ell^\pm$  branching fractions typically fix a relatively precise location in  $(m_{1=2}; \tan \beta)$  parameter space. These values can be compared to those required by the  $m_{A^0}$  and  $m_{\tilde{e}_1}$  mass measurements. Consistency within experimental errors is typically only possible for a small set of closely related models. In the sample situation detailed in Section 4, where we assumed that one of the six GUT models was correct and computed statistical errors on that basis, only one of the remaining five models could possibly be confused with the input model after measuring the above three branching fractions relative to that for the final state used for tagging. By subdividing the SUSY signal into final states with a definite number of leptons and any number of jets, and considering as well the  $H^0 \rightarrow h^0 h^0$ ,  $A^0 \rightarrow Z h^0$  and  $H^\pm \rightarrow W^\pm h^0$  branching fractions, we found it possible to distinguish between these two choices at a very substantial statistical level. Thus, a unique model among the six rather similar models is singled out by combining measurements from the Higgs sector with those from conventional SUSY pair production. In short, measurements deriving from pair production of Higgs particles can have a great impact upon our ability to experimentally determine the correct SUSY GUT model.

The above discussion has left aside the fact that for universal soft-scalar masses the measured value of the slepton mass would determine the relative magnitude of  $m_0$  and  $m_{1=2}$ . Of the two models mentioned just above, one has a large  $m_0 = m_{1=2}$  value and the other a much smaller value. They could be easily distinguished on the basis of  $m_\ell$  alone. However, if the soft-scalar slepton mass is not the same as the soft-scalar Higgs field masses at the GUT scale, the branching fraction ratios would give the best indication of the relative size of the soft-scalar Higgs mass as compared to  $m_{1=2}$ .

More information regarding the slepton/sneutrino mass scale and additional ability to discriminate between models are both realized by subdividing the SUSY decays of the Higgs bosons in a way that is sensitive to the relative branching fractions for slepton/sneutrino vs. chargino/neutralino decays. Slepton/sneutrino channels essentially only produce leptons in the final state, whereas the jet component is typically larger than the leptonic component for chargino/neutralino decays (other than the totally invisible  $\tilde{e}_1^0 \tilde{e}_1^0$  mode). Thus, we are able to define individual SUSY channels, characterized by a certain number of leptons and/or jets, which display a strong correlation with the slepton/sneutrino decay component. We find that these individual channels have sufficiently large event rates that the ratios of the branching fractions for these channels can typically be determined with reasonable statistical precision. For the earlier-mentioned input model, we can compute the statistical level at which the other five GUT scenarios would be ruled out using various of these ratios of branching fractions. Excellent discrimination between models on this basis is found.

---

<sup>8</sup>Only the average can be determined given that typically  $m_{A^0} \neq m_{H^0}$ .

In conclusion, our study shows that not only will detection of Higgs pair production in  $e^+e^-$  or  $pp$  collisions (at planned luminosities) be possible for most of the kinematically accessible portion of parameter space in a typical GUT model, but also the detailed rates for and ratios of different neutral and charged Higgs decay final states will very strongly constrain the choice of GUT-scale boundary conditions. In estimating experimental sensitivity for Higgs pair detection and for measuring Higgs masses and branching fractions, we included substantial efficiencies and all relevant branching fractions. Although we believe that our estimates are relatively conservative, it will be important to re-visit this analysis using a full Monte Carlo detector simulation.

## 6 Acknowledgements

This work was supported in part by Department of Energy under grant No. DE-FG03-91ER40674 and by the Davis Institute for High Energy Physics. We wish to thank C.H. Chen for making his evolution program available to us.

## References

- [1] P. Langacker and M. Luo, Phys. Rev. D 44 (1991) 817; U. Amaldi, W. de Boer and H. Furstenau, Phys. Lett. B 260 (1991) 447; J. Ellis, S. Kelley and D. Nanopoulos, Phys. Lett. B 260 (1991) 131.
- [2] See J.F. Gunion, H.E. Haber, G.L. Kane and S. Dawson, The Higgs Hunters Guide, Addison-Wesley Publishing, and references therein.
- [3] J.F. Gunion, A. Stange, and S. Willenbrock, Weakly-Coupled Higgs Bosons, preprint UCD-95-28 (1995), to be published in Electroweak Symmetry Breaking and New Physics at the TeV Scale, edited by T.L. Barklow, S. Dawson, H.E. Haber, and J.L. Siegrist (World Scientific, Singapore, 1996).
- [4] J.F. Gunion, J. Kelly, and J. Ohnemus, Phys. Rev. D 51 (1994) 2101.
- [5] A. Djouadi, J. Kalinowski, P. Ohm ann and P.M. Zerwas, hep-ph/9605339.
- [6] Proceedings of the First Workshop on the Physics Potential and Development of  $pp$  Colliders, Napa, California (1992), Nucl. Instru. and Meth. A 350, 24 (1994); Proceedings of the Second Workshop on the Physics Potential and Development of  $pp$  Colliders, Sausalito, California (1994), ed. by D. Cline, American Institute of Physics Conference Proceedings 352; Proceedings of the 9th Advanced ICFA Beam Dynamics Workshop: Beam Dynamics and Technology Issues for  $pp$  Colliders, Montauk, Long Island, (1995), to be published.
- [7] J.F. Gunion and H.E. Haber, Phys. Rev. D 37 (1988) 2515.

- [8] For a review and references, see A.B. Lahanas and D.V. Nanopoulos, Phys. Rep. 145 (1987) 1.
- [9] A. Brignole, L.E. Ibanez, and C. Munoz, Nucl. Phys. B 422 (1994) 125, Erratum, *ibid.*, B 436 (1994) 747. See also V.S. Kaplunovsky and J. Louis, Phys. Lett. B 306 (1993) 269.
- [10] G. Anderson, D. Castano, Phys. Rev. D 52, 1693-1700 (1995).
- [11] H. Baer, F. Paige, S. Protopopescu, and X. Tata, in Proceedings of the Workshop On Physics at Current Accelerators and Supercolliders, eds. J. Hewett, A. White, and D. Zeppenfeld, Argonne National Laboratory (1993).
- [12] We thank C.H. Chen for making his program available to us.
- [13] H. Baer, J.F. Gunion, C. Kao, and H. Pois, Phys. Rev. D 51 (1995) 2159.